AGU PUBLICATIONS

JGR

Journal of Geophysical Research: Atmospheres

RESEARCH ARTICLE
10.1002/2016JD025694

**Key Points:**
- The stronger precipitation and runoff was mainly located over India, Indochina-southeast China with elasticity values greater than 2
- The elasticity between precipitation and runoff are dominated with positive signals, indicating positive P-ROF relationship
- Runoff process is influenced by initial soil conditions, where soil moisture has higher influence than initial soil temperature conditions

**Supporting Information:**
- Supporting Information S1

**Correspondence to:**
A. K. Mishra,
ashokm@g.clemson.edu

**Citation:**
Liu, D., A. K. Mishra, and K. Zhang (2017), Runoff sensitivity over Asia: Role of climate variables and initial soil conditions, *J. Geophys. Res. Atmos.*, *122*, 2218–2238, doi:10.1002/2016JD025694.

Received 23 JUL 2016
Accepted 11 FEB 2017
Accepted article online 15 FEB 2017
Published online 24 FEB 2017



# Runoff sensitivity over Asia: Role of climate variables and initial soil conditions

**Di Liu[1,2], Ashok K. Mishra[2], and Ke Zhang[1,3,4]**

[1]College of Hydrology and Water Resources, Hohai University, Nanjing, China, [2]Glenn Department of Civil Engineering, Clemson University, Clemson, South Carolina, USA, [3]State Key Laboratory of Hydrology-Water Resources and Hydraulic Engineering, HoHai University, Nanjing, China, [4]Cooperative Institute for Mesoscale, Meteorological Studies, University of Oklahoma, Norman, Oklahoma, USA

**Abstract** We applied statistical and numerical modeling approach to evaluate the sensitivity of runoff (ROF) to climate variables using Global Land Data Assimilation System (GLDAS) data and regional climate model (RegCM4). It was observed that ROF is more sensitive to precipitation (P) compared to other analyzed hydroclimatic variables (potential evapotranspiration (PET), 2 m air temperature (T2m), solar radiation (Rn), specific humidity (SSH), and wind speed (U), especially over India, Indochina, and south-north-northeast China semihumid-humid climate transition zones based on the higher correlation coefficient (>0.7) and elasticity (>2). The abnormal positive T2m-ROF observed over Tibetan Plateau region (TP) may be due to its high topography and cold weather regime, while positive PET-ROF over India and north China-southeast Mongolia regions can be attributed to the stronger influence of local land-atmosphere interactions. Soil moisture (SM) reflects high correlation with runoff, especially over the climate transition zones (i.e., India and Indochina-southeast China). The initial wet (dry) soil moisture (SM) anomalies lead to an increase (decrease) of ROF in each season with the hot spots mainly located in middle to high latitudes (spring), TP and northeast (summer and autumn), and Indochina (autumn) regions. Such influence can persist almost 4 months in spring while only about 1 month in autumn during dry and wet conditions. The wet condition has stronger influence at beginning but dissipates quickly, while the dry condition can last longer within the same season. The impact of initial soil temperature anomalies on ROF is weaker than SM, with the only obvious ROF changes located over south China (spring and summer) and north India (autumn).

## 1. Introduction

Climate change has become increasingly significant in the past several decades [*Intergovernmental Panel on Climate Change,* 2007a, 2007b], which likely to alter spatiotemporal distribution of rainfall as well as water resources. Good management of water resources is critical for providing reliable source of water for domestic consumption, food production, and ecosystems that rely on surface and ground water. Therefore, assessing the impacts of climate change on the hydrological cycle is important to improve water resource management. However, the challenge is to measure the rate of changes in hydrologic variables in space and time. For example, long-term average runoff depends largely on climatic conditions and is expected to change as climate change progresses, but to what degree and in which locations is uncertain [*Donohue et al.*, 2011]. The spatial characteristics of runoff (ROF) sensitivity, while important from a management perspective, are currently poorly understood.

The partitioning of precipitation into actual evaporation and runoff can be used as the simple water balance equation when evaluating the trend in annual evaporation or runoff for the long term. However, the regional water balance depends on hydroclimatic conditions and is affected by land surface factors. The key issue in annual water balance at the catchment scale is how to estimate actual evaporation from potential evaporation. As highlighted in previous literatures [e.g., *Koster and Suarez*, 1999; *Yang et al.*, 2006], the actual evaporation and potential evaporation have complementary relationship due to the connections and feedbacks between water-energy balances and the landscape. [*Budyko*, 1974] assumed that actual evaporation is controlled by both water and energy availabilities. At the annual timescale, the water availability is the amount of annual precipitation and the energy availability can be measured by the potential evaporation. Therefore, in the "Budyko hypothesis," the runoff changes are assumed to be sensitive to the changes in precipitation and evapotranspiration. However, *Arnault et al.* [2016], *Bouchet* [1963], *Brubaker and Entekhabi* [1996], *Dirmeyer* [2011], *Guo et al.* [2006], *Koster et al.* [2011], *Koster et al.* [2006], *Liu et al.* [2015, 2014a, 2014b], and

*Seneviratne et al.* [2010] indicated that the changes of terrestrial conditions (e.g., soil moisture, soil temperature, and runoff) would also exert certain impact on the subsequent changes of climate variables (e.g., precipitation and surface air temperature) due to land-atmosphere interactions.

In the past decades, the sensitivity of runoff to climate changes or terrestrial changes was assessed by both statistical analysis method [e.g., *Brikowski*, 2015; *Chiew*, 2006; *Huang and Yang*, 2015; *Potter and Chiew*, 2011; *Seager et al*., 2009; *Vano et al*., 2012; *Xu et al*., 2013a; *Yang and Yang*, 2011] and numerical modeling method [e.g., *Arnault et al*., 2016; *Schaake et al*., 1996; *Yang et al*., 2000]. These findings demonstrates that the runoff changes are sensitive not only to the precipitation but also to other hydroclimatic variables, including surface air temperature, solar radiation, wind speed, specific humidity, and soil conditions (soil moisture, soil cracks, and soil temperature). For example, *Dooge et al.* [1999] indicated that the runoff elasticity depends on many factors, including the stochastic nature of climate, field capacity of soils, soil moisture levels, length of soil water depletion, saturated hydraulic conductivity, and the humidity ratio. *Sankarasubramanian and Vogel* [2003] demonstrated the role of soil moisture storage in the determination of long-term water balance. *Nunes et al.* [2009] reported the high sensitivity of storm runoff and peak runoff rates to changes in storm rainfall and soil water content in Mediterranean watersheds. *Li et al.* [2012] indicated the effects of shrinkage soil cracks in the runoff processes and found that the spatial heterogeneity of runoff generation mechanisms was highly dependent upon the strength (intensity and depth) of the rainfall events and antecedent soil moisture conditions. In a recent study, *Konapala and Mishra* [2016] investigated the performance of a three-parameter streamflow elasticity model as a function of hydrologic fluxes, such as precipitation, potential evaporation, and change in groundwater storage applicable at both seasonal and annual scales in 245 Model Parameter Estimation Experiment basins spread across the continental USA.

This study aims to investigate the sensitivity of runoff to the climate change over Asia. The large spatial variations in both physiographic characteristics and climate type over Asia result in a large variation in the hydrologic response to climate variability and change. Many studies highlighted the changes in runoff and climatic factors in many different regions of Asia. For example, *Yang et al.* [2014] found a reduction of precipitation occurred in the Hai River Basin, the upper reach of the Yangtze River Basin, and the Yellow River Basin, while an increase occurred in the western China. *Liu et al.* [2014] indicated 29% decline of surface wind speed in China during 1966 to 2011, resulted in 1–6% increase in runoff and 1–3% decrease in evapotranspiration at most regions in China. In addition, most of the river basins in north China witness a decline in mean annual runoff, such as the Shiyang River Basin [*Ma et al*., 2008], the Yellow River Basin [*Cong et al*., 2009; *Tang et al*., 2007], and the Hai River Basin [*Ma et al*., 2010]. The sensitivity of runoff to climate changes was evaluated in few river basins. For example, *Yang and Yang* [2011] found that the climate elasticity of runoff (e.g., the elasticities of runoff to precipitation and/or potential evapotranspiration) was sensitive to the catchment characteristics in the Hai River basin and Yellow River basin of China.

Two kinds of methods are applied in this study to quantify the sensitivity of runoff to climate changes. First, multiple statistical analysis are used to characterize the signatures of hydrologic variability over the study area and to investigate the complex interacting processes that contribute to the runoff responses. The concept of separating the effects of different hydroclimatic variables (e.g., precipitation, 2 m air temperature, soil moisture, and soil temperature) on runoff are discussed in previous literatures [e.g., *Brikowski*, 2015; *Huang and Yang*, 2015; *Sankarasubramanian and Vogel*, 2003; *Yang and Yang*, 2011]. Second, the numerical modeling is conducted to provide physical insights into the mechanisms or processes, which might have led to the estimated hydrological signature patterns. The Global Land Data Assimilation System (GLDAS) data version 2 from Noah land surface model [*Rodell et al*., 2004] is adopted to provide the long-term hydroclimatic data time series. We applied regional climate model (RegCM4 coupled with CLM3.5) [*Elguindi et al*., 2011; *Giorgi et al*., 2012; *Steiner et al*., 2009] developed by the Abdus Salam International Center for Theoretical Physics to investigate the possible influence of predominant soil conditions on the subsequent changes of runoff.

The structure of the remaining paper are as follows: the data and study area are described in section 2; the methodologies, including the multiple statistical analysis and the numerical modeling experimental design with RegCM4 are introduced in section 3; the statistical results are explained in section 4, while the numerical modeling results are illustrated in section 5; and the conclusions are summarized in section 6.

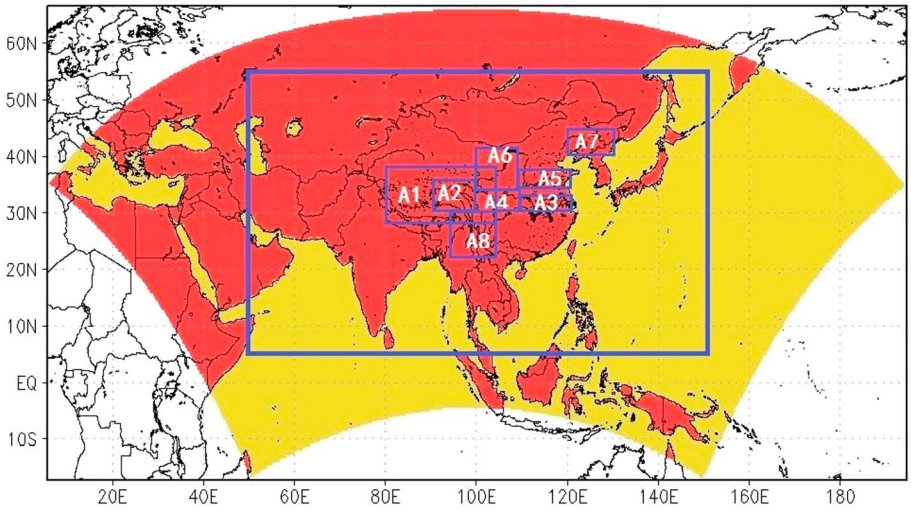


**Figure 1.** The RegCM4 domain (shaded) and study area (within blue frame) over (5–55 N, 50–150 E). The eight subregions contain the main river basin: (A1) TP region; (A2) TP River Basin; (A3) middle-lower Yangtze-Huai River Basin; (A4) upper Yangtze-Huai River Basin; (A5) Lower Yellow River Basin; (A6) upper Yellow River Basin; (A7) north-east River Basin; and (A8) south-east Zhujiang River Basin.

## 2. Data and Study Area

Due to the lack of long-term observed data over the study domain, we used the 0.25° × 0.25° monthly GLDAS-2 data set from 1948 to 2007 (http://disc.sci.gsfc.nasa.gov/services/grads-gds/gldas) to provide the hydroclimatic variables, such as precipitation, 2 m air temperature, evapotranspiration, runoff, soil moisture, and soil temperature. The GLDAS data are proved to agree well with the data (precipitation and 2 m air temperature) from the University of East Anglia Climate Research Unit (CRU) version TS3.1 not only in the spatial pattern but also in the magnitude from the annual and seasonal mean and/or standard deviation of precipitation and 2 m air temperature in our previous studies [*Liu et al*., 2015, 2014a, 2014b]. In this study, the soil moisture and soil temperature data within top 1 m depth are used because these variables are considered most vital in the land-atmosphere interactions according to *Liu et al.* [2015, 2014a, 2014b].

The RegCM4 is used to investigate the impact of predominant soil conditions on the subsequent changes of runoff. The modeling domain and study area (5–55 N, 50–150 E) (within the blue frame) derived from RegCM4 are given in Figure 1, which covers most part of Asia and its adjacent regions. To better illustrate the sensitivity of runoff to the climate changes, eight subregions along the main river basins (within the blue region marked with white labels from A1 to A8 in Figure 1) are selected: (A1) TP region, (A2) TP River Basin, (A3) middle-lower Yangtze-Huai River, (A4) upper Yangtze-Huai River Basin, (A5) lower Yellow River Basin, (A6) upper Yellow River Basin, (A7) north-east River Basin, and (A8) south-east Pearl River Basin. The details about the latitude and longitude scope of each region and the number of grid cells are given in Table 1.

The hydroclimatic variables used in this paper are abbreviated as follows: potential evaportranspiration (PET), net radiation (Rn), 2 m air temperature (T2m), specific humidity (SSH) and wind speed (U), precipitation (P), evapotranspiration (ET), runoff (ROF), soil moisture (SM), and soil temperature (ST).

## 3. Methodologies

### 3.1. Hydroclimatic Indices

Multiple hydroclimatic indices, including the aridity index (AI), runoff ratio (ROFR), and runoff variability ratio (ROFV) defined in *Sankarasubramanian and Vogel* [2003], are selected to investigate the sensitivity of runoff to climate changes using GLDAS data. Here the AI, ROFR, and ROFV (defined as the hydroclimatic indices) are used to evaluate the long-term hydroclimatic characteristics over the study area. As defined in *Sankarasubramanian and Vogel* [2003], AI is the ratio of mean annual potential evapotranspiration to mean annual precipitation, ROFR is the ratio of mean annual runoff to mean annual precipitation, and ROFV is

**Table 1.** Description of the Eight Selected Subregions: (A1) TP Region; (A2) TP River Basin; (A3) Middle-Lower Yangtze-Huai River Basin; (A4) Upper Yangtze-Huai River Basin; (A5) Lower Yellow River Basin; (A6) Upper Yellow River Basin; (A7) North-East River Basin; (A8) South-East Zhujiang River Basin[a]

| Index | Subregions | Latitude | Longitude | Grid Cells |
|---|---|---|---|---|
| A1 | TP | 28–38°N | 80–105°E | 4000 |
| A2 | TP River Basin | 30–35°N | 90–100°E | 800 |
| A3 | Middle-lower Yangtze-Huai River basin | 30–33°N | 110–120°E | 480 |
| A4 | Upper Yangtze-Huai River basin | 30–35°N | 105–110°E | 400 |
| A5 | Lower Yellow River basin | 35–37°N | 110–120°E | 320 |
| A6 | Upper Yellow River basin | 35–42°N | 100–110°E | 1120 |
| A7 | North-east River basin | 40–45°N | 120–130°E | 800 |
| A8 | South-east Pearl River basin | 22–30°N | 95–105°E | 1280 |

[a]The number of grid cells are the total grid cells over each region, including the "NaN" values over the water covered area. It is calculated with latitude equation (−7.625: 0.25: 64.375) and longitude equation (34.375: 0.25: 155.375).

the ratio of standard deviation of annual runoff to the standard deviation of annual precipitation. The AI index is categorized into humid (magnitude within 0–0.33), semihumid (magnitude within 0.33–1), temperate (magnitude within 1–2), semiarid (magnitude within 2–3), and arid (magnitude within 3–7), to simply represent the water resources conditions.

In this study, we adopted the maximum possible evaporation concept used in Evald Oldekop's work addressed in *Andréassian et al.* [2016] and *Ol'dekop* [1911] (equaled maximum evaporation to net radiation in the original Budyko scheme) and approximated PET with the sum of latent heat flux (abbreviated as LH (unit: W/m$^2$)) and sensible heat flux (abbreviated as SH (unit: W/m$^2$)) using the equation PET ≈ (LH + SH)/$\lambda$, where $\lambda$ is the latent heat of vaporization of water (unit: J/kg) and $\lambda \approx 2.5 * 1E6$. To make it simple, the precipitation contains both the rainfall and snowfall while the runoff is derived from the total surface runoff and subsurface runoff. The additional discussion on snow component used in GLDAS product can be found in available literatures [*Livneh and Lettenmaier*, 2010; *Mitchell*, 2001; *Rodell and Houser*, 2004; *Rodell et al.*, 2004]. The detailed concept on snow component and frozen soils within CLM3.5 model can be referred to *Oleson et al.* [2007, 2008]. The impact of snow or snow melting water on the subsequent runoff changes is not considered separately.

### 3.2. Trend Analysis

Two commonly used nonparametric methods, Mann-Kendall (MK) [*Kendall and Gibbons*, 1990] and Sen's slope estimator [*Sen*, 1968] were applied to quantify the significance of trends in hydroclimatic time series. The Mann-Kendall test is used to detect the presence of trend, while the magnitude of trend is estimated by the Sen's slope calculated with equation (1):

$$\beta = \text{median}\left[\frac{(X_j - X_j)}{(j - i)}\right]. \quad (1)$$

$X_j$ and $X_i$ are the hydroclimatic time series (e.g., precipitation) at the $i$th or $j$th decade. For all $i < j$, where $\beta > 0$ indicates an increasing trend and $\beta < 0$ indicates a decreasing trend. The magnitude of $\beta$ indicates the steepness of the trend.

The Mann-Kendall statistical test ($Z_S$) is estimated at the specific $\alpha$ significance level. When $|Z_S| > Z_{1-\alpha/2}$, the null hypothesis is rejected and a significance trend exists in the time series. $Z_{1-\alpha/2}$ is obtained from the standard normal distribution table. In this study, significance level $\alpha = 0.05$ is used. The Mann-Kendall and Sen's methods have been widely used in the hydroclimatic time series [*Chattopadhyay and Edwards*, 2016; *Gocic and Trajkovic*, 2013; *Tabari and Hosseinzadeh Talaee*, 2011; *Mishra and Singh*, 2010; *Mishra et al.*, 2011; *Taxak et al.*, 2014].

### 3.3. Nonparametric Estimator of Elasticity

The correlation coefficient is used as a statistical measure to make inferences about the degree of association between variables [*Khed et al.*, 2012]. The advantage of correlation coefficient is to represent the relationship

between two variables; however, it may not evaluate the influence of rate of changes in one variable would exert on the other. The elasticity index can be used to supplement such disadvantage.

The concept of elasticity was introduced to the hydrological literature by *Schaake* [1990] to quantify the sensitivity of runoff to changes in climate. It is broadly quantified with two methods: statistical method [*Brikowski*, 2015; *Sankarasubramanian and Vogel*, 2003; *Zheng et al*., 2009] and the theory-based analysis method (e.g., Budyko hypothesis [*Sankarasubramanian et al*., 2001; *Schaake*, 1990; *Yang and Yang*, 2011]).

Due to the simple calculation, the statistical method has been greatly used in the P-ROF feedback analysis [*Brikowski*, 2015; *Sankarasubramanian and Vogel*, 2003]. This method, also called nonparametric elasticity, is defined as proportional change in runoff to the proportional change in a climatic variable such as precipitation. Given adequate historical record, the elasticities $\varepsilon$ can be obtained from a statistical description (median over time) of observed annual values of elasticity with equation (2):

$$\varepsilon_X = \text{median}\left[\frac{(R_i - \overline{R})/\overline{R}}{(X_i - \overline{X})/\overline{X}}\right]. \tag{2}$$

where $R_i$ is the runoff for the $i$ th time period (usually water year), $X_i$ is the climate or watershed variable of interest (e.g., P and PET) for the $i$ th time period, and $\overline{X}$ is the long-term average of that variable. The simplest of these expressions includes only precipitation elasticity ($\varepsilon_p$), typically the largest contribution to elasticity.

This nonparametric estimator of elasticity was used to derive the elasticity of runoff to precipitation and other climate variables (i.e., T2m ($\varepsilon_T$), PET ($\varepsilon_{PET}$), Rn ($\varepsilon_{Rn}$), SSH ($\varepsilon_{SSH}$), and wind ($\varepsilon_U$)) to separate the contributions of different climatic variables on runoff. The results are illustrated in section 4.4. The elasticity derived from *Zheng et al.* [2009] (named as Zheng's elasticity for short) and the "Budyko-type formulation" given in *Yang and Yang* [2011] (named as Yang's elasticity for short) are also discussed for a comparison.

### 3.4. Numerical Modeling With RegCM4

The numerical modeling with RegCM4 conducted in our previous studies [*Liu et al*., 2015, 2014a, 2014b] is chosen here to further assess the response of runoff to the predominant soil conditions (i.e., initial soil moisture or soil temperature). The model is set with a 50 km horizontal resolution, 18 vertical levels, CLM3.5 land surface scheme, and the MIT-Emanuel convection scheme with the domain centered at (30°N, 100°E), consisting of 264 (west to east) × 150 (south to north) grid points (Figure 1, shaded area). The lateral boundary adopts the National Centers for Environmental Prediction/National Center for Atmospheric Research Reanalysis Project version 2 data [*Kalnay et al*., 1996; *Kanamistu et al*., 2002], while the sea surface temperature forcing uses the Met Office Global Sea Ice and Sea Surface Temperature data [*Rayner et al*., 2006]. The simulations from the sensitivity experiments conducted earlier [*Liu et al*., 2015, 2014b] are adopted in this paper to investigate the impact of initial soil moisture or soil temperature anomalies on the changes of subsequent runoff. The initial control run is set for 20 years continuously during 1991–2010 periods. The details of the RegCM4 model, model validation, and the sensitivity experimental design can be found in *Liu et al.* [2015, 2014a, 2014b] and briefly described in the supporting information. The numerical modeling results with RegCM4 are discussed in section 5.

## 4. Results and Discussion

### 4.1. Spatial Pattern of Hydroclimatic Indices

The spatial patterns of AI, ROFR, and ROFV derived from the long-term data during 1948–2007 are plotted in Figure 2. As shown, the AI exhibits an obvious spatial gradient across the study area, highlighting the spatial gradients of aridity. The semiarid to arid regions mainly locating in the northwest China, southwest Mongolia, and the west regions over the middle to high latitudes present semiarid to arid climatic pattern, while the southeast to northeast study area adjacent to the ocean shows temperate to semihumid to humid climatic pattern in the annual timescale. This compares well with the land use and vegetation type (Figure S5), the arid regions almost located over the areas with semidesert or desert or ice cap/glacier (northwest China-southwest Mongolia and west middle- to high-latitude regions), the temperate regions with crop/mixed farming, short grass, or evergreen needle leaf tree, and the semihumid-humid regions mixed with woodland, forest, irrigated crop, and inland water. The arid-semiarid regions correspond with higher elevation and

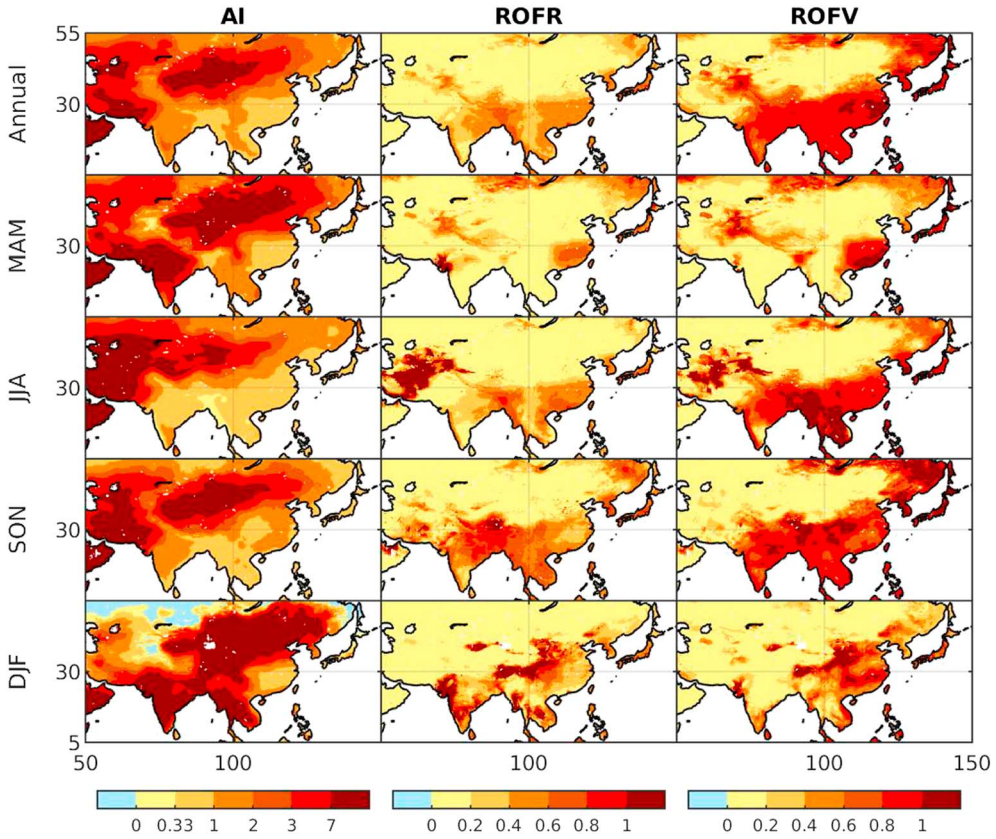


**Figure 2.** Spatiotemporal patterns of hydroclimatic indices during the study period (1948–2007) at the annual (annual) and seasonal (spring (MAM), summer (JJA), autumn (SON), and winter (DJF)) timescales: (AI) aridity index; (ROFR) runoff ratio; (ROFV) runoff variability ratio.

topography, while the semihumid-humid regions are with flat topography (within 500 m or 1000 m surface elevation) (Figures S6 and S7).

By comparison, the arid regions have lower ROFR than the semihumid-humid regions, implying that as the AI value decreases, the ROFR increases. The higher ROFR is mainly located over the India and Indochina-southeast China with complex topography and rivers. As stated in [*Sankarasubramanian and Vogel*, 2003], the ROFR likely to be high in hilly regions with substantial cloud cover that in turn decreases the incoming short-wave radiation and increases long-wave radiation from clouds, thereby decreasing the net radiation available at the Earth's surface for evaporation. The spatial patterns of ROFV agree well with the ROFR, also exhibiting higher ROFV over the India, Indochina-southeast China, and northeast study regions. The higher ROFV implies the stronger response of runoff to the changes of precipitation variability. The lower ROFV magnitude over the arid regions is due to the limited moisture as the changes in P tend to produce roughly equal changes in actual ET, which results in negligible changes in ROF. In contrast, the high ROFV magnitude over the humid basins presents that the ET does not act to buffer ROF in these regions as it does in arid and semiarid regions. Over the southeast China region, the ROFV are greater than 1. As documented in *Sankarasubramanian and Vogel* [2003], if the ROFV is greater than 1, the aridity condition may be likely due to the feedback effect. In the case of humid basins, a positive P anomaly due to increased cloud cover will further reduce the net radiation available at the surface, resulting in a negative correlation between P and ET, and therefore leads to the increased positive anomalous ROF. *Sankarasubramanian et al.* [2001] pointed out that the Budyko hypothesis can only explain variations of streamflow elasticity to precipitation for very humid regions where the moisture and energy balance are in phase with one another. *Yang et al.* [2006] indicated that the changes of actual evaporation in nonhumid regions is dominated by change in precipitation rather than potential evaporation, while actual evaporation is controlled by change in potential evaporation than precipitation in humid regions change. *Koster and Suarez* [1999] also highlighted runoff variability based

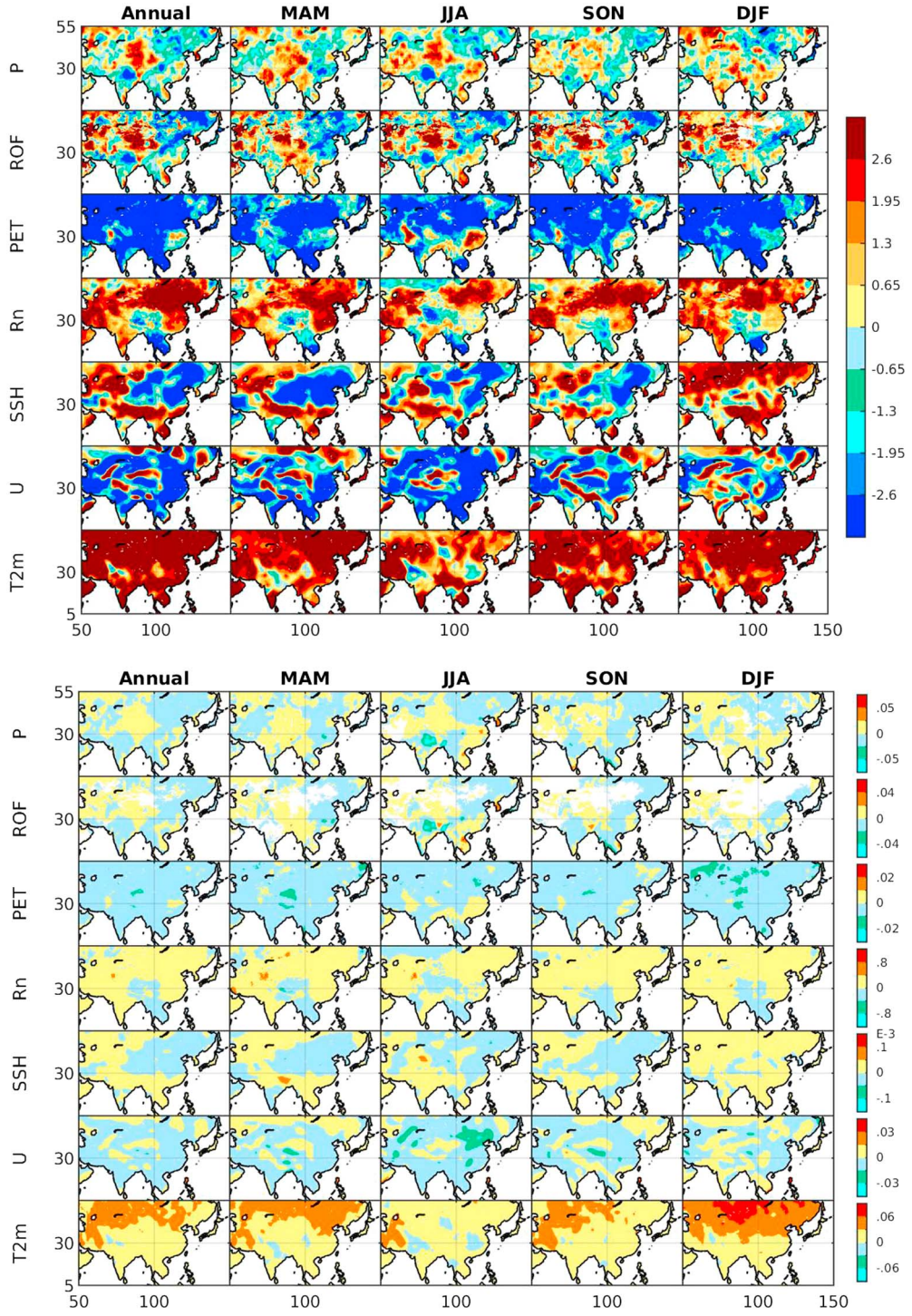


**Figure 3.** (top) The Mann-Kendall test ($Z_S$) results for yearly precipitation (P), runoff (ROF), potential evapotranpiration (PET), net radiation (Rn), surface specific humidity (SSH), wind speed (U), and 2m air temperature (T2m) during the study period (1948–2007) at the annual (Annual) and seasonal (spring (MAM), summer (JJA), autumn (SON), and winter (DJF)) timescales. If $|Z_S| > 1.96$ indicated the data time series passed the 5% significance level with significant trend, while if $|Z_S| > 2.576$ passed the 1% significance level with significant trend. (bottom) The Sen's slope estimator for yearly precipitation (P), runoff (ROF), potential evapotranspiration (PET), net radiation (Rn), surface specific humidity (SSH), wind speed (U), and surface air temperature (T2m) time series during the study period (1948–2007) at the annual (Annual) and seasonal (spring (MAM), summer (JJA), autumn (SON), and winter (DJF)) timescales.

on the Budyko hypothesis [*Budyko,* 1974], which suggested that the strength of land-atmosphere feedback is strongly related to the relative availability of local energy and water.

The seasonal spatial patterns seem to be similar with the annual timescale over most part of the study area except over some typical regions. As shown in Figure 2, the water resources over the inland (northwest China-southwest Mongolia) mainly come from the summer (June–August (JJA)) season, the monsoon regions (India-Indochina) from summer (JJA) and autumn (September–October (SON)) seasons, and the midwest regions from winter season (December–February (DJF)). Such differences mainly come from the climate regime in different seasons. For example, the India, Indochina, north China-northeast China, and southeast Mongolia regions have less precipitation in winter and spring seasons to summer and autumn seasons, leading to the temperate (Indochina in spring) or arid water conditions, combined with lower ROFR and ROFV. By comparison, the hotspots (e.g., North India, Indochina, and southeast China) diagnosed by ROFV (magnitude greater than 1) as strong feedback regions in spring, summer, and autumn seasons are consistent to the hotspots investigated with strong land-atmosphere coupling strength in previous studies [e.g., *Koster et al*., 2006; *Liu et al*., 2014b; *Zhang et al*., 2011]. Over these regions, the changes of terrestrial and atmospheric variables (e.g., SM, ST, ROF, P, T2m, and ET) would influence each other according to the two-way land-atmosphere feedbacks stated in *Brubaker and Entekhabi* [1996], *Entekhabi et al.* [1992], and *Seneviratne et al.* [2010]. Our previous work [*Liu et al*., 2015, 2014a] diagnosed strong SM/ST-atmosphere coupling strength over the climate transition zones (i.e., North India and southeast China in summer season especially for SM/ST-T2m) over Asia, and such feedback can enlarge the climate pattern (e.g., precipitation endurance and intensity, and surface air temperature) and climate extremes (e.g., drought, cold days, hot days, and heat wave) over these areas [*Liu et al*., 2014b].

### 4.2. Temporal Pattern of Hydroclimatic Indices

The annual and seasonal Mann-Kendall statistical test ($Z_S$) and Sen's slope estimator ($\beta$) of decadal P, ROF, PET, Rn, SSH, U, and T2m during 1948–2007 years are plotted in Figure 3 (top and bottom), respectively. Positive values of $Z_S$ indicate increasing trends, vice versa for the negative $Z_S$ values.

As shown, the signals from the Mann-Kendall test (Figure 3, top) and Sen's slope estimator (Figure 3, bottom) almost share similar positive or negative spatial patterns in both the annual and seasonal timescale. According to the Mann-Kendall test, the precipitation trend did not pass the 5% significance test over most of the study area ($|Z_S|$ is lower than 1.96 at most grids). Even though, it presents insignificant decreasing trend over North India (summer and autumn), North Indochina (summer and autumn), and north-northeast China (each season) around the Tibetan Plateau (TP) region while an insignificant increasing trend over the inland regions, including TP (each season), northwest China-southwest Mongolia (each season), and part of South India, South Indochina, and southeast China in spring and winter, with the magnitude of Sen's slope within [−0.025, 0.025] mm/d (year$^{-1}$). By comparison, most of the increased P is located over the arid regions. The annual changes of P over the southeast China, including the middle-lower Yellow River Basin, middle-lower Yangtze River Basin, and Pearl River Basin, are mainly due to changes in spring and summer seasons, while the annual P changes over India and Indochina regions are mainly from summer and autumn seasons. Sen's slope over these regions seems to be greater than 0.05 mm/d (year$^{-1}$). Consistent with the findings in *Huang and Yang* [2015], the P has an increasing trend in the northwest China, while a decreasing trend in the Yellow River Basin, Hai River Basin, and the upper reaches of Yangtze River Basin over the north China region. The Sen's slope for runoff has similar spatial patterns and resembles similar magnitude with P over most part of the study area in the annual and seasonal timescale.

Unlike P and ROF, the annual or seasonal PET has a significant decrease trend over the past decades over most part of the study area in both the annual and seasonal timescale with an exception over the southeast and northeast China (summer and autumn) where the Sen's slope shows an insignificant increasing trend. Such increased signal may be caused by the strong land-sea-atmosphere interactions over these areas explained in *Brubaker and Entekhabi* [1996] and *Koster and Suarez* [1999]. According to the Budyko Hypothesis, the sensitivity of runoff can be approximated by the changes in precipitation and potential evapotranspiration, where potential evapotranspiration can be approximated with the function of climatic variables (Rn, U, SSH, and T2m) based on Penman's equation. As shown, the Rn has significant increased trend in the annual or seasonal timescale over most part of the study area with an exception over Indochina-Tibetan Plateau region. The SSH has a mixed significant increasing and decreasing annual or seasonal

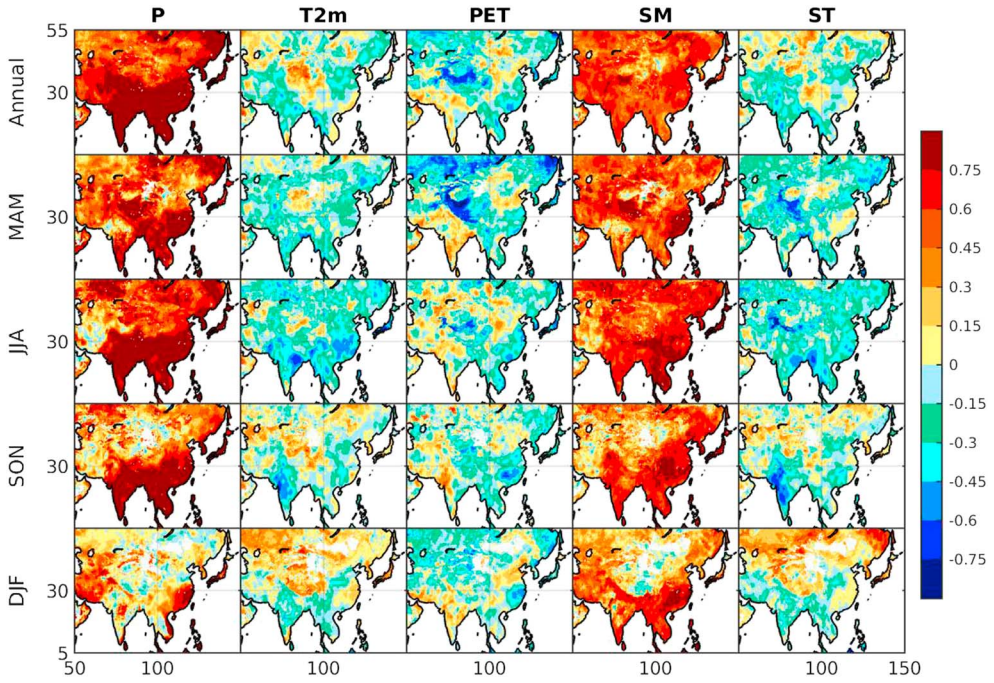


**Figure 4.** Grid-based annual or seasonal correlation between runoff (ROF) and precipitation (P), 2m air temperature (T2m), potential evapotranspiration (PET), soil moisture (SM), or soil temperature (ST) during the study period (1948–2007).

trends: where the increasing trend is mainly located over the India, Indochina-south China, and west part of study area, while the decreasing trend is located over the TP and north China-northeast China-southeast Mongolia region. The U showed significant decreasing trend over most part of the study area in spring and summer. The T2m has a significant increasing trend over the past decades over most part of the study area, especially over the middle-high latitudes above 30° in spring, autumn, and winter seasons where the trend slopes are greater than 0.03 K/yr. The trends of these hydroclimatic variables indicated by the Sen's slope and Mann-Kendall statistical test indicators are almost consistent with the findings in *Huang and Yang* [2015] over China. It can be observed that trends (Figure 3, top) and magnitude (Figure 3, bottom) of increasing or decreasing slopes for runoff and climate variables are different. There is no clear pattern in terms of trend (magnitude) associated between climate variables and corresponding runoff. This indicates a complex (inconsistent) relationship that exists between runoff and climate variables. Among these variables, the spatial pattern and magnitude of runoff remain consistent with precipitation, representing the vital role of precipitation in the runoff changes. The significant increasing trend of T2m indicates the global warming and climate changes in the past decades.

### 4.3. Correlation Between Hydroclimatic Variables

The annual and seasonal correlation between runoff and precipitation is calculated to illustrate the sensitivity of runoff to precipitation (Figure 4). As shown in Figure 4, the correlation between runoff with current year precipitation is dominantly positive with the higher magnitude (greater than 0.72) located over the India, Indochina, and southeast China regions at annual as well as spring, summer, and autumn seasons.

The correlation strength of P-ROF processes has a gradually increasing trend from the north to the south of study area, and the arid-semiarid to semihumid-humid regions in both the annual and seasonal timescale. Additionally, the regions with high correlation magnitude in each season also have higher ROFV (magnitude greater than 1), indicating possible stronger land-atmosphere interactions. The remaining study area, including the northwest China, southwest Mongolia, northwest study area, TP and its adjacent regions, has lower correlation values, implying weak P-ROF correspondence due to the complex topography and land type (mainly desert and glacier) as the less precipitation and arid water conditions prevents the amount of water to form runoff.

According to water balance theory, the total precipitation potentially equals to the amount of ROF and ET for a long period of time. In this way, the ET and ROF have a negative relationship. *Budyko* [1974] assumed that actual ET is controlled by both water and energy availabilities. At the annual timescale, the water availability is the amount of annual P and the energy availability can be measured by the PET. As highlighted in previous literatures (e.g., [*Koster and Suarez*, 1999; *Yang et al*., 2006]), the actual evaporation and potential evaporation has complementary relationship due to the connections and feedbacks between water-energy balances and the landscape. Disregarding the indirect effects of T2m on ROF (e.g., causal or associative relationships between regional rainfall and changing temperatures), the only way increasing T2m can influence ROF in a calibrated rainfall-runoff model is through consequent changes in PET. The interactions of decreased PET with increased annual rainfall are likely to generate additional ROF. This is because the decrease of PET leads to comparatively increased SM, and so increase of rainfall is more likely to result in more ROF generation. To further assess the sensitivity of ROF to climate changes, the correlation between ROF with current year T2m, PET, SM and ST are separately calculated (Figure 4).

As expected, the correlation of T2m-ROF is dominated with negative signals over most part of the regions (including India, Indochina, and southeast China-northeast China) with significant runoff trend in the annual timescale or each seasonal timescale. Over these regions, the increase of T2m would increase ET, which would reduce the amount of water generating ROF. Over the TP regions and the high latitude with cold weather regime, the increase of T2m, would cause melting of snow or ice, resulting in the increase of water supply to ROF, thus reflecting positive correlation of T2m-ROF, especially in autumn and winter season.

The correlation between PET and ROF are negative over most part of the study area except the India and north China-southeast Mongolia regions over the climate transition zones (semihumid temperate or even to arid transition), where the positive PET-ROF relationship may be caused by the local climate feedback. As stated in *Koster et al.* [2006], *Liu et al.* [2014b], and *Zhang et al.* [2011], both India and north China-southeast Mongolia has strong land-atmosphere coupling strength, where the changes of terrestrial variables (e.g., soil moisture or soil temperature) would exert obvious influence on the subsequent local climate variables (e.g., precipitation and surface air temperature) according to the land-atmosphere feedback mechanisms stated in *Brubaker and Entekhabi* [1996], *Entekhabi et al.* [1992], *Koster et al.* [2006], *Seneviratne et al.* [2010]. The ET plays an important role in the linkage of SM and precipitation in the land-atmosphere interactions. Based on the positive land-atmosphere interactions, the increased SM would lead to a cascading effect including the increase of ET, decrease of T2m, and an increase of P. *Koster and Suarez* [1999] indicated the possibility of land-atmosphere feedback in the complex relationship among runoff, precipitation, and evapotranspiration based on Budyko hypothesis [*Budyko,* 1974]. Therefore, the increased P may lead to the increase of ROF. In this notation, the ET has a positive relationship with P, which would lead to a positive relationship to ROF. In our previous studies [*Liu et al*., 2014a, 2014b], we found that the SM exhibits positive relationship with ET over most part of the study area in each season: northwest middle-high latitudes (summer), north India and north China (spring, summer, and autumn seasons), and Indochina in spring season. The positive correlation between ROF and ET is within these hot spots in each season.

Neglecting the weak or negative signals over the TP-northwest China and southwest Mongolia regions in winter or autumn seasons, the SM-ROF correlation is positive over most part of the study area in each season, especially over the India-Indochina-southeast China regions. This is reasonable according to the storage of SM and the strong land-atmosphere interactions over these regions. By comparison, the spatial patterns of SM-ROF are consistent with the P-ROF, demonstrating the importance of SM over the regions with significant P-ROF feedback. In addition, the hot spot (i.e., the south China in spring, Indochina in summer, southeast China in autumn and winter) with higher SM-ROF correlation also has higher ROFV (Figure 2).

Unlike the positive SM-ROF correlation, the ST-ROF are primarily negative over most part of the study area during the annual, spring, and summer timescales, reflecting a negative ST-ROF relationship, while the ST tends to be positive with ROF in autumn over the high latitude when the weather tends to be cold which resulted in the reduction of ROF. The magnitude of ST-ROF correlation over the south study area, especially India, is higher, reflecting the possible stronger relationship between ST and ROF. According to the water and energy balance, the ET would likely to increase with increased ST, which would finally lead to the decrease in ROF. In winter, when the weather tends to be cold, the ST-ROF is likely to be dominated with positive signals.

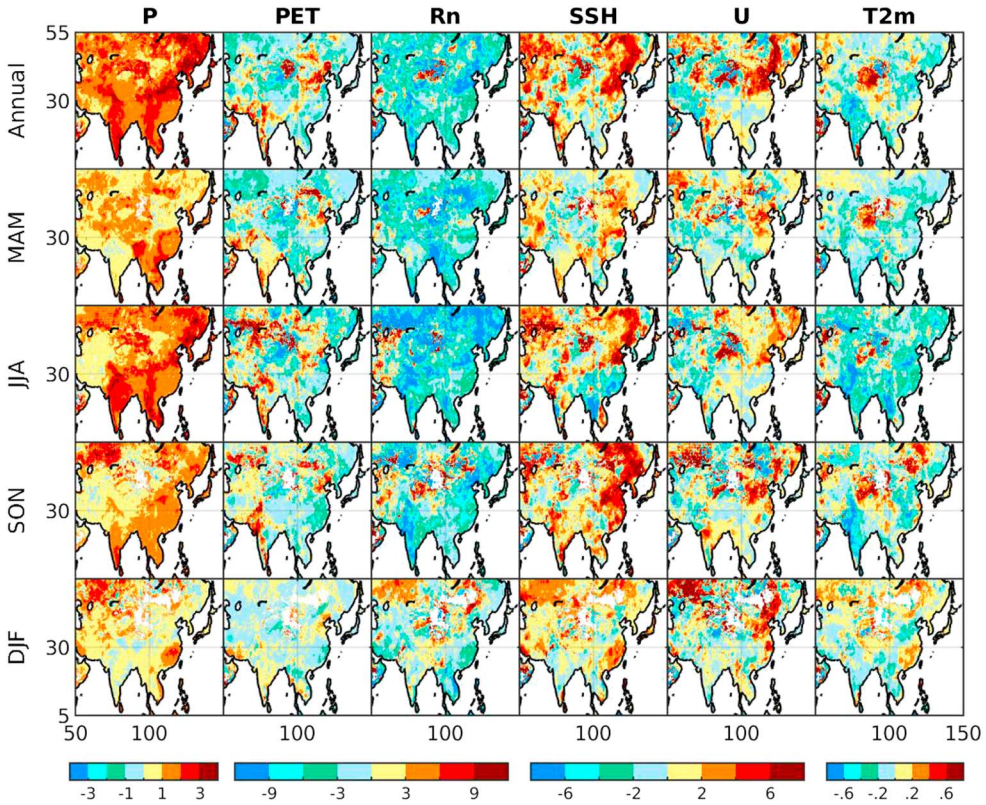


**Figure 5.** Runoff (ROF) elasticity to precipitation (P), potential evapotranspiration (PET), net radiation (Rn), surface specific humidity (SSH), wind speed (U), and 2 m air temperature (T2m) during the study period (1948–2007) at the annual (Annual) and seasonal (spring (MAM), summer (JJA), autumn (SON), and winter (DJF)) timescales according to equation (2).

The increase of ST would result in the melting of ice and snow and increase in ROF, but the influence is not strong according to the lower magnitude of the correlation coefficient.

### 4.4. Relationship Between Runoff Elasticity and Hydroclimatic Variables

The elasticity of ROF to P ($\varepsilon_P$) derived with equation (2) at different timescales are shown in Figure 5. Clearly, the spatial patterns of $\varepsilon_P$ compare well with their correlation patterns. The grid-based annual or seasonal $\varepsilon_P$ is positive over most part of the study area, implying a positive P-ROF response process. As shown in Figure 5, the magnitude of $\varepsilon_P$ is greater than 1 during the annual or summer timescale over most part of the study area, implying the changes of 1% P would result in more than 1% changes of ROF. The $\varepsilon_P$ over the climate transition zones, including India, Indochina, north-northeast China (middle-lower reaches of Yellow-Yangtze River Basin), is higher with magnitude greater than 2 during the annual and summer timescale. In spring, autumn, and winter season, the elasticity of ROF to P would be influenced by the cold weather, especially over the middle to high latitudes with arid water conditions and complex topography, where the elasticity magnitude is reduced, reflecting the weak influence of precipitation on the changes of ROF. Some previous literatures [e.g., *Sankarasubramanian et al.*, 2001; *Risbey and Entekhabi*, 1996] highlighted the cold weather scheme (i.e., snowpack storage) and buffered the impact of climate change on local annual streamflow.

The runoff elasticity with respect to other variables, including PET ($\varepsilon_{PET}$), Rn ($\varepsilon_{Rn}$), SSH ($\varepsilon_{SSH}$), wind ($\varepsilon_U$), and T2m ($\varepsilon_T$) are also given in Figure 6. Clearly, the spatial patterns of $\varepsilon_{PET}$ agree well with the correlation patterns of ROF with PET. The signals are negative over the Indochina-southeast China while positive over the India and north-northeast China in the annual timescale and each season. The spatial grids with higher ($\varepsilon_{PET}$) magnitude also have higher ($\varepsilon_P$) magnitude. The $\varepsilon_{Rn}$ is negative over most part of the study area during both the annual and seasonal timescale. The $\varepsilon_{SSH}$ and $\varepsilon_U$ are dominated with positive signals, while $\varepsilon_T$ is dominated with negative signals over most part of the study area, especially over the India and north-northeast China regions.

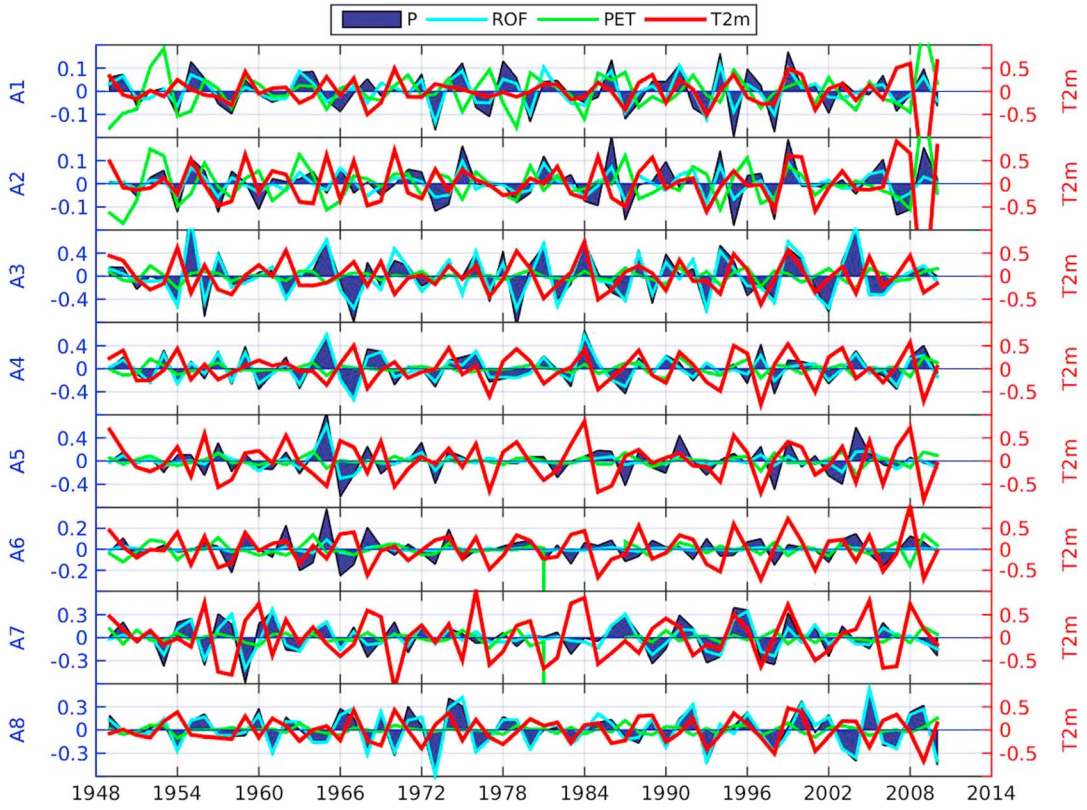


**Figure 6.** Time series of annual runoff (ROF) versus precipitation (P), Potential Evapotranspiration (PET), and 2m air temperature (T2m) over the eight subregions (A1–A8).

Over India and north China-northeast China regions witness significant change in ROF, where P, PET, SSH, and U exert positive contributions to the changes of ROF, while Rn and T2m provide negative contributions to the changes of ROF assessed by the elasticity. Unlike the smaller magnitude of $\varepsilon_{Rn}$, $\varepsilon_{SSH}$, or $\varepsilon_U$ stated in other studies [*Huang and Yang*, 2015; *Yang and Yang*, 2011], the magnitude indicated in this study has higher values, [−9, 9] for $\varepsilon_{Rn}$, [−2, 2] for $\varepsilon_{SSH}$ and $\varepsilon_U$, and [−0.6, −0.2] for $\varepsilon_T$ over these regions. For the Indochina-south China regions, the P contributes a positive impact to the changes of ROF with $\varepsilon_P$ within [1, 3], while the PET, Rn, and T2m has a negative influence on ROF with elasticity values within [−3, 0], [−6, 0], and [−0.4, −0.2], respectively. This difference may be caused by the difference in methodologies and modeling uncertainties.

The elasticity results from Zheng's method [*Zheng et al*., 2009] and Yang's method [*Yang and Yang*, 2011] are provided for comparison study (Figures S8 and S9). Clearly, the results from Zheng's method differ little with the results from equation (2). They not only resemble the same spatial patterns but also share similar magnitude for runoff elasticity to each climate variable at the same timescale. The results from Yang's method are almost consistent with the two statistical methods over most of the study area except the arid regions (northwest China-southwest Mongolia region and western part of study area) where the signals of ROF elasticity to P are negative in the annual timescale and spring, autumn, and winter seasons, implying that the Budyko hypothesis about the ROF elasticity to P may not apply in certain conditions. As highlighted in *Sankarasubramanian et al*. [2001], the Budyko hypothesis can only explain the variations in precipitation elasticity of streamflow for very humid basins. Even though, all methods agreed that India, Indochina, and south-north-northeast China are the regions with strong P-ROF processes. The $\varepsilon_{PET}$ is negative over these regions with magnitude within [−1.8, −0.6]. The $\varepsilon_{Rn}$ is positive over the India region with magnitude above 1.2 while negative over the southeast China with magnitude within [−1.8, 0], while $\varepsilon_{SSH}$ is negative over the India region but positive over the southeast China with magnitude within [−1.5, 1.5]. The $\varepsilon_U$ is negative over the India-Indochina regions while positive over the north China with magnitude within [−1.5, 1.5]. The $\varepsilon_T$ is positive over the India-Indochina regions while negative over the north China with magnitude within [−0.1, 0.1]. The difference between the Yang's method with our approach may be due to difference in theory of each

method. Yang's method is based on Budyko's hypothesis, as the data used here are from modeling output. It may contain some uncertainties, and results would rely on the correctness of the rainfall-runoff model used to generate the PET.

Compared to previous studies at catchment scale with observed data, the runoff elasticity to precipitation from each method agrees well with previous studies over the same study area. For example, *Huang and Yang* [2015] assessed the climate elasticity of runoff to the climatic factors over 207 catchments in China. They found that the precipitation elasticity ranged from 1.1 to 4.75 (2.0 on average) over the whole catchments with the lowest value ranged from 1.1 to 1.5, occurred in southern China, while the highest value occurred in the north-northeast China regions, including Huai River Basin, Liao River Basin, the Hai River Basin, and the lower reach of Yellow River Basin. Our findings agree well with these studies, demonstrating the efficiency of GLDAS data in this study. In addition, *Yang et al.* [2014] also indicated that the precipitation elasticity to be 1.1 to 4.8 in China, which is similar to our findings. Moreover, the $\varepsilon_P$ was also calculated in previous studies and found to be 2.6 in the Luan River Basin in north China [*Xu et al*., 2013b] and 1.0 to 2.0 over the catchment of the Pearl River Basin in southeast China [*Jiang et al*., 2007; *Wang et al*., 2013]. Those results were also in good agreement with our results for the precipitation elasticity in the same regions.

### 4.5. Evaluation of Runoff Elasticity at Regional Scale

We selected eight typical subregions located over the main river basin in China to further investigate the sensitivity of runoff to climate changes. Over each subregion, the annual time series of P, ROF, and PET versus T2m as well as the time series of ROF versus SM or ST are used to illustrate the relationships between runoff and these climate variables. The moving average filter method is used to remove the oscillation. The correlation and elasticity are given to illustrate the sensitivity of runoff to climate changes over each region.

As shown in Figure 6, the trend of runoff has a positive relationship with precipitation while negative with T2m and PET. The SM reflects a positive feedback to the runoff at most time periods while negative to the ST in the annual timescale (Figure 7). The correlation coefficients between current year precipitation and runoff is positive over the eight subregions in the annual timescale with the magnitude higher than 0.6, demonstrating a positive relationship of precipitation with runoff (Table 2, correlation coefficient). Consistently, the yearly runoff elasticity to the current year precipitation is positive over each subregion, with the values within [1.4, 3.5] (Table 2, elasticity), demonstrating the nonlinear relationship of P-ROF due to the change in storage response within the study area.

To better illustrate the sensitivity of runoff to climate variables, the box plots at the annual and seasonal timescale are provided for a quantitative analysis. The box plots of the elasticity of ROF to P derived from the grid cells over each subregion at the annual and seasonal temporal scales are shown in Figure 8. It is observed that: the elasticity of runoff to P indicates positive signals at annual and seasonal timescales over each region. The mean of runoff elasticity to P (median values from box plots) based on the grids located within each subregion at the annual timescale is above 2 at most subregions except A1 and A6 (values $>$ 1). The mean runoff elasticity magnitude at the summer timescale is comparatively higher in comparison to other seasons, while these values are low at the winter timescale (almost close to 0). The mean runoff elasticities at spring season is comparatively low in comparison to summer and autumn season at some of the subregions (A4: upper Yangtze-Huai River Basin, A5: lower Yellow River Basin, A6: upper Yellow River Basin, and A7: north-east River Basin) located over the middle to high latitudes where cold weather regime also expected in spring season. The difference in mean magnitude of runoff elasticities at different seasons implies the variability in sensitivity of runoff at different seasons. The outliers in some of the regions (i.e., A1, A2, and A6) imply the possible large variation among runoff elasticities in those study regions. This may be attributed to topography, wide difference between local to regional climate, uneven contribution of meteorological forcing on runoff, and difference in number of grids within the study area. For example, A1 region contains the most part of Tibetan Plateau, which has complicated topography that lead to the uneven response of runoff to precipitation with in grid cells. However, most of the outliers (i.e., A1 (spring, autumn, and winter)) are above the maximum signal, indicating higher elasticity of runoff to precipitation. In addition, the outliers in most regions in spring, autumn, and winter seasons are stronger than that in summer, possibly indicating the complicated sensitivity of runoff to precipitation in these seasons.

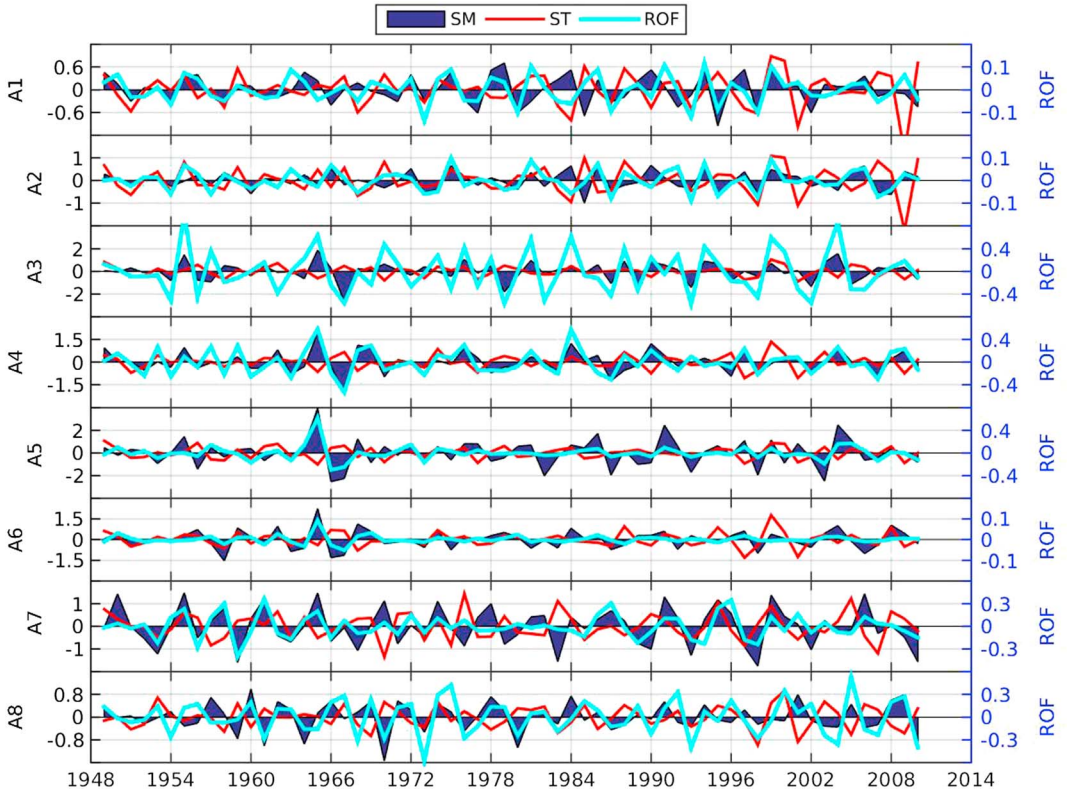


**Figure 7.** Time series of annual runoff (ROF) versus soil moisture (SM) or soil temperature (ST) over the eight subregions (A1–A8).

The correlation between runoff with current year T2m, PET, and SM is provided in Table 3 to analyze the influence of other climate variables on runoff. As shown, the T2m exerts negative signals over most of the subregions except over the regions in cold weather regime (e.g., TP (A1) and TP river basin (A2) in the annual correlation, autumn and winter). The PET shows negative signals over most of the subregions (except A4

**Table 2.** Correlation Coefficient and Runoff (ROF) Elasticity With Respect to Current Year Precipitation (P) Over the Eight Subregions Described in Table 1[a]

| Index | Subregions | Year | MAM | JJA | SON | DJF |
|---|---|---|---|---|---|---|
| Correlation coefficient | A1 | 0.88 | 0.89 | 0.84 | 0.67 | 0.04 |
| | A2 | 0.87 | 0.85 | 0.82 | 0.45 | 0.02 |
| | A3 | 0.93 | 0.86 | 0.88 | 0.81 | 0.51 |
| | A4 | 0.93 | 0.78 | 0.79 | 0.85 | 0.22 |
| | A5 | 0.80 | 0.50 | 0.70 | 0.66 | *-0.08* |
| | A6 | 0.65 | 0.31 | 0.49 | 0.46 | *-0.11* |
| | A7 | 0.89 | 0.47 | 0.89 | 0.64 | 0.23 |
| | A8 | 0.96 | 0.84 | 0.84 | 0.86 | 0.29 |
| Elasticity | A1 | 1.74 | 1.70 | 2.28 | 0.80 | *-0.01* |
| | A2 | 2.49 | 1.35 | 2.22 | 0.81 | 0.19 |
| | A3 | 2.32 | 1.85 | 1.41 | 1.60 | 0.73 |
| | A4 | 2.76 | 1.43 | 1.68 | 1.65 | 0.13 |
| | A5 | 2.63 | 0.53 | 2.79 | 1.39 | 0.18 |
| | A6 | 1.41 | 0.28 | 1.01 | 1.22 | 0.03 |
| | A7 | 3.43 | 1.10 | 2.96 | 1.31 | 0.30 |
| | A8 | 2.17 | 1.49 | 2.02 | 1.31 | 0.34 |

[a]The MAM, JJA, SON, and DJF are abbreviated for spring season (March, April, and May), summer season (June, July, and August), autumn season (September, October, and November), and winter season (December, January, and February), respectively. The italic numbers present negative correlation coefficient or elasticity.

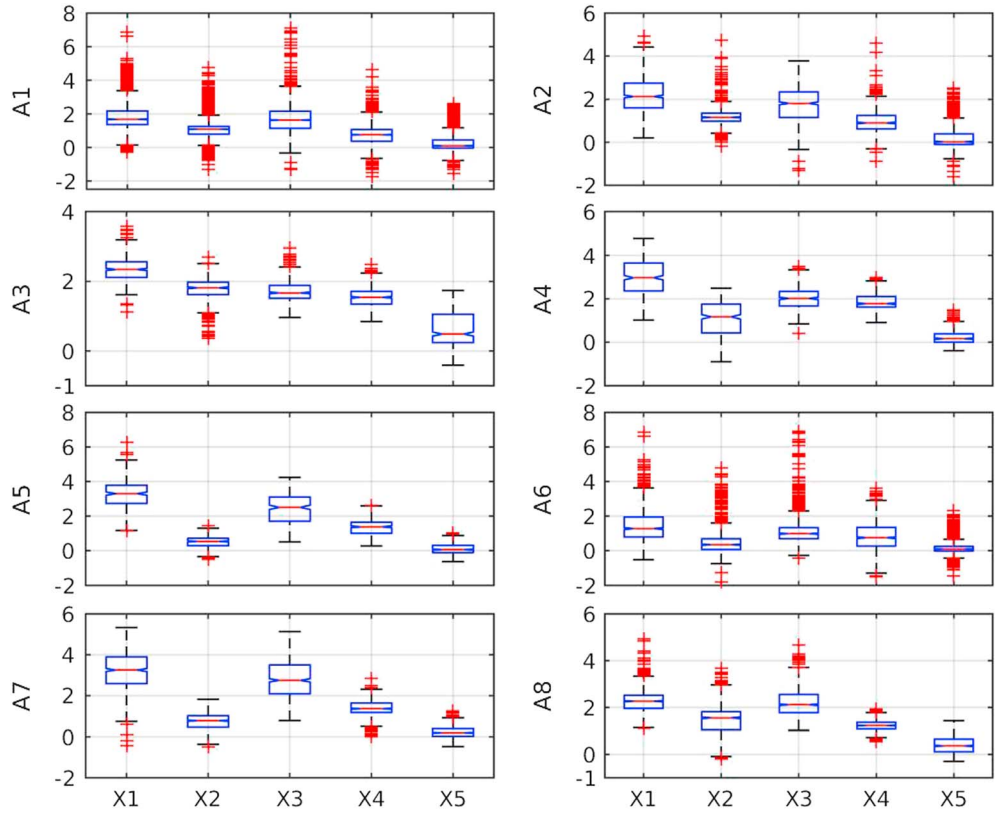


**Figure 8.** Box plot of runoff (ROF) elasticity to precipitation (P) over the eight subregions at the annual and seasonal timescale during the study period (1948–2007). A1 to A8 represent eight selected subregions shown in Figure 1. X1 to X5 in the *X* axis present the timescale for annual, spring (MAM), summer (JJA), autumn (SON), and winter (DJF), respectively.

in the annual timescale, A5 in spring, A4 and A6 in summer) though the magnitude is not high (lower than 0.5 in most cases). The SM reflects positive and high magnitude (above 0.6 in most regions in each season), implying the positive SM-ROF feedback. The magnitude of the correlation of T2m or PET with runoff is much lower compared to the correlation between precipitation (or soil moisture) with runoff, implying the less influence of T2m and PET in the changes of runoff under climate change. The precipitation and soil moisture stand out as the main factor in the runoff changes over the subregions.

## 5. Numerical Modeling Results Analysis

### 5.1. Impact of Initial Soil Moisture Anomalies on Runoff Analysis

Based on the mechanism of land-atmosphere interactions, the dry SM would lead to a decrease of ET while an increase of T2m, finally causing a decrease of precipitation. Due to the positive P-ROF relationship, the decreased precipitation would finally result in the decrease of runoff. Therefore, the decrease in soil moisture would lead to the decrease of runoff. The wet SM anomalies would lead to the reverse cascade effects leading to increase in runoff. As expected, the initial dry SM anomalies lead to a decrease of runoff, while the initial wet anomalies lead to an increase of runoff in spring (March–May (MAM)), summer (JJA), and autumn (SON) season (Figure 9). According to previous studies [e.g., *Koster et al.*, 2006; *Liu et al.*, 2015, 2014a, 2014b], the land-atmosphere coupling strength is weak in winter. The correlation and elasticity results in this study also indicate weak sensitivity of runoff to the hydroclimatic variables in winter season (i.e., regional results presented in section 4.5). Therefore, only three seasons, spring, summer, and autumn seasons, are considered. The findings are documented and explained as follows.

During spring season, the influences of initial SM anomalies on the subsequent runoff were mainly located over the middle to high latitudes (above 30°N) in both the dry and wet conditions. Such influence can persist for almost 4 months. Due to the initial dry SM condition, the influence on the subsequent runoff is not strong during the initial 14 days to 1 month compared to the following months due to the cold weather regime in

**Table 3.** Correlation Coefficient Between Runoff (ROF) With Current Year 2m Air Temperature (T2m), Potential Evapotranspiration (PET) and/or Soil Moisture (SM) Over the Eight Subregions[a]

| | Year | MAM | JJA | SON | DJF |
|---|---|---|---|---|---|
| | | | *T2m* | | |
| A1 | 0.20 | 0.12 | *−0.01* | 0.26 | 0.36 |
| A2 | 0.32 | *−0.09* | *−0.01* | 0.34 | 0.39 |
| A3 | *−0.20* | *−0.20* | *−0.54* | *−0.03* | 0.09 |
| A4 | *−0.34* | *−0.16* | *−0.47* | *−0.17* | *−0.30* |
| A5 | *−0.28* | *−0.31* | *−0.21* | *−0.16* | *−0.11* |
| A6 | *−0.32* | *−0.10* | *−0.35* | *−0.17* | 0.03 |
| A7 | *−0.22* | *−0.44* | *−0.22* | 0.03 | 0.11 |
| A8 | *−0.01* | *−0.22* | *−0.45* | 0.02 | *−0.29* |
| | | | *PET* | | |
| A1 | *−0.18* | *−0.65* | *−0.11* | *−0.16* | *−0.14* |
| A2 | *−0.28* | *−0.54* | *−0.35* | *−0.25* | *−0.16* |
| A3 | *−0.23* | *−0.39* | *−0.39* | *−0.35* | *−0.34* |
| A4 | 0.01 | *−0.08* | 0.04 | *−0.31* | 0.10 |
| A5 | *−0.00* | 0.23 | *−0.09* | −0.25 | 0.26 |
| A6 | *−0.06* | *−0.09* | 0.38 | −0.07 | 0.09 |
| A7 | *−0.06* | *−0.10* | *−0.25* | *−0.17* | *−0.02* |
| A8 | *−0.12* | *−0.41* | *−0.19* | *−0.26* | 0.01 |
| | | | *SM* | | |
| A1 | 0.55 | 0.84 | 0.52 | 0.48 | 0.19 |
| A2 | 0.65 | 0.71 | 0.70 | 0.63 | *−0.11* |
| A3 | 0.72 | 0.85 | 0.83 | 0.78 | 0.76 |
| A4 | 0.77 | 0.65 | 0.77 | 0.85 | 0.63 |
| A5 | 0.77 | 0.67 | 0.77 | 0.77 | 0.40 |
| A6 | 0.62 | 0.39 | 0.62 | 0.58 | 0.30 |
| A7 | 0.70 | 0.51 | 0.80 | 0.82 | 0.49 |
| A8 | 0.54 | 0.68 | 0.82 | 0.79 | 0.72 |

[a]The italic numbers present negative correlation coefficient.

the early spring. During the early spring, the SM in the cold weather regime has a limited role to exert land-atmosphere interactions; meanwhile, the ET from the surface vegetation or snow surface is likely to have higher influence with atmosphere interactions. Therefore, the cold weather minimizes the impact of SM on the local climate. Later on, as time goes, the weather tends to be warmer; the SM starts to be active in the local land-atmosphere interactions, which would increase its impact on the local runoff. As shown, the impact of initial SM anomalies during the wet condition seems to start at an early stage compared to the dry condition, but it also dissipates quicker, especially over TP-southeast China and northeast study regions. During spring when the weather gets warmer, the water from snowmelt would feed the soil, which would prolong the soil moisture conditions, thus resulting in longer consistent influence on the subsequent climate variables, including runoff. The increased SM would also provide increased subsurface runoff.

In summer season, the initial dry SM anomalies lead to the decrease of runoff, while the wet anomalies cause an increase of runoff over TP, Indochina, and northeast study regions. The impact of initial wet SM anomalies is quicker (higher magnitude) compared to the dry SM anomalies, but it also dissipates quickly. As shown, the influence during the dry condition can persist for almost 3 months over the Indochina region while about 4 months over the middle to high latitudes (above 30°N), while such influence can persist only 1 month in the wet condition.

During autumn season, the influence from the dry SM condition is weak compared to summer season with the only obvious signals exit over TP and part of the northeast study area. The wet condition has obvious influence over the south China, TP, and northeast China regions. Such influence can last about 1 month in both the dry and wet conditions, which may be caused by the cold weather regime in the late autumn season. While weather turns cold, the impact of SM on local climate would be reduced according to the frozen soil water, thus shortening the persistence influence on the local runoff.

### 5.2. Impact of Initial Soil Moisture Anomalies on Hydroclimatic Variables

To better understand the causal relationship between initial SM anomalies with the subsequent ROF, the influence of initial SM anomalies on subsequent surface ROF, subsurface ROF, P, ET, T2m, Rn, SSH, and U was also analyzed (Figures S10–S17 in the supporting information). As shown, the dry SM anomalies lead to the decrease in both surface ROF and subsurface ROF, while the wet anomalies hold the reverse influence in each season. The spatial patterns of surface ROF agrees well with the subsurface ROF, though the influence of initial SM anomalies on surface ROF is weak compared to the subsurface ROF. This is reasonable based on the SM-ROF mechanism. The wet SM would need less P to get saturated, which would lead to more water available for surface ROF. The response of P to initial SM anomalies is weak and scattered. Even though, the wet SM anomalies lead to increase P, while the dry anomalies diminish P in each season. The spatial patterns of P are consistent with the ROF over most part of the study area with an exception over the Indochina region in summer

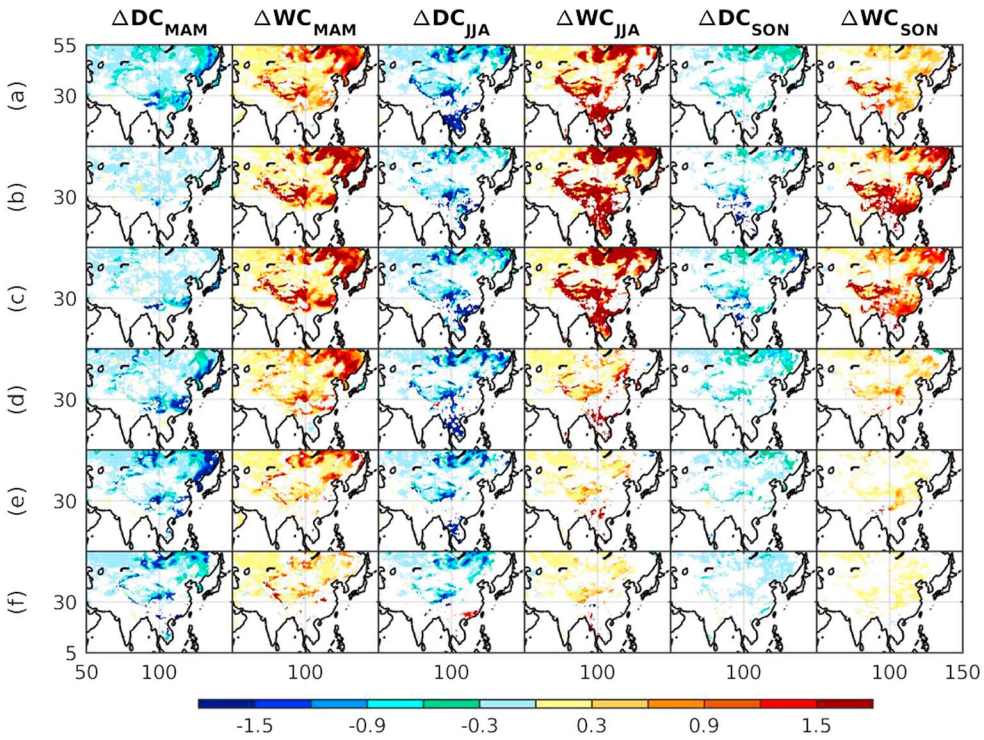


**Figure 9.** Differences of averaged daily total runoff (ROF) (mm/d) between the dry and control condition (ΔDC) or between the wet and control condition (ΔWC) in spring (MAM), summer (JJA), and autumn (SON) seasons; (a–f) the averaged results in the first 3 months, the first 14 days, first month, second month, third month, and fourth month, respectively, in each season. Only the areas with values passing the 10% significance test are shaded.

season. The changes in ROF over Indochina region are significant and spatially continuous in summer, while the changes of P are quite weak and spatially scattered. This may be caused by the local large scale circulation anomalies instead of the land-atmosphere interactions [*Liu et al*., 2014b].

The increase of ET would lead to possible decrease in ROF. The wet SM anomalies lead to the increase of ET, vice versa for the dry SM anomalies. The regions with strong SM-ET response but weak SM-ROF feedback may be due to the local land-atmosphere interactions; the changes of SM would mainly result in the changes of ET, while over the regions with weak land-atmosphere interaction, the changes in SM would likely to alter the local water balance based on the changes of ROF. Previous literatures [e.g., *Koster and Suarez*, 1999; *Sankarasubramanian et al*., 2001; *Yang et al*., 2006] highlighted the relationship among P, ROF, and ET and the influence of land-atmosphere feedback on this complicated relationship.

The spatial patterns of T2m agree well with the change of ET in each season with the same SM condition. In addition, the regions with significant changes of SSH and U are also within the regions with significant changes of ET, indicating the relationship between ET, T2m, SSH, and U. The increase in SM anomalies leads to the increase of ET, decrease of T2m and U, and increase of SSH. The decreased SM anomalies hold the reverse reactions in each season. The changes of Rn are weak and scattered. Even though, the wet SM anomalies lead to the increase in Rn over most part of the study area with an exception over Indochina which has opposite changes, while the dry anomalies hold the reverse influence in each season.

By comparison, the regions with obvious responses of runoff to the initial SM anomalies are within the regions with significant SM-ROF correlation stated in section 4.3. The SM-ROF has positive correlation over the India-Indochina-southeast China regions in each season. These regions are also with significant precipitation-runoff processes, indicating the role of precipitation and soil moisture in the changes of runoff. The responses of runoff to ET, Rn, SSH, U, and T2m are consistent with the runoff elasticity to ET, Rn, SSH, U, or T2m, respectively.

### 5.3. Impact of Initial Soil Temperature Anomalies on Runoff Analysis

Compared to the SM anomalies, the influence of ST anomalies on runoff is weak and they were scattered during both conditions, i.e., colder or warmer anomalies (Figure 10). Even though, the warmer ST anomalies lead

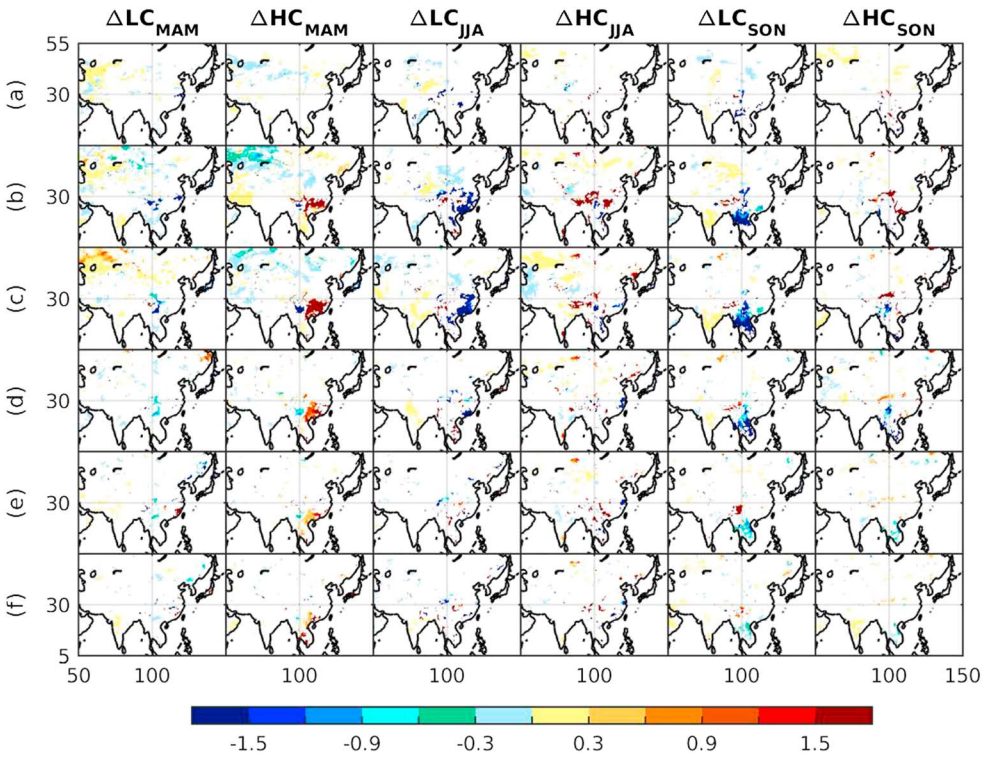


**Figure 10.** Changes of total runoff (mm/d) mean between the colder and control conditions (ΔLC) or between the warmer and control conditions (ΔHC) in spring (MAM), summer (JJA), and autumn (SON) seasons. (a–f) indicate the averaged results in the first 15 days, second 15 days, third 15 days, fourth 15 days, fifth 15 days, and sixth 15 days in each season. Only the results that passed the 10% significance test are shaded.

to the increase of runoff, while the colder anomalies diminish the runoff over part of the north Indochina to south China regions in some of the seasons (Figure 10). These regions also witness significant changes in precipitation (Figure S18). During spring, the signals of runoff change are witnessed over the south China in warmer condition. Such responses can last for about 45 days. In summer, the significant signals are located over south China region and can last for 30 days, while in autumn, the significant signals exist over the north Indochina region during the cold ST conditions and can last for almost 45 days. Over these hot spots, the warmer ST anomalies lead to increased P (over 4 mm/d) (Figure S18), increased ET ($<$0.5–1 mm/d) (Figure S19), increased T2m (Figure S20), increased SSH ($>$0.003 kg/kg) (Figure S21), decreased U (quite weak) (Figure S22), and Rn (Figure S23), while the colder ST anomalies hold the reverse conditions. The influence of initial ST anomalies on the initial SM anomalies varies in space and time, and the influence of ST on the subsequent hydroclimatic variables is weak compared to SM.

## 6. Conclusions

This study aims to investigate the sensitivity of runoff to climate variables over Asia using both statistical and RegCM4 numerical modeling methods. The correlation and nonparametric elasticity values are used to evaluate the sensitivity of runoff to the hydroclimatic variables (e.g., P, T2m, PET, and SM). A group of sensitivity experiments with RegCM4 is conducted to assess the impact of initial soil moisture and soil temperature anomalies on runoff.

As analyzed, the higher sensitivity of runoff to the climate variables are mostly located over the India, Indochina, and south-north-northeast China regions in semihumid-humid climatic conditions. The following conclusions can be drawn from this study:

1. Runoff is more sensitive to precipitation in comparison to other hydroclimatic variables (e.g., T2m and PET). The spatial pattern and magnitude of temporal trends of runoff agree well with precipitation among the hydroclimatic variables. Both the correlation and elasticity between precipitation and runoff are

dominated with positive signals, indicating positive P-ROF relationship. The runoff elasticity to precipitation is within the range of [1, 3.5] over most part of the study area, implying the nonlinear relationship between runoff and precipitation. The changes in 1% precipitation would result in 1%–3.5% changes of runoff. The major P-ROF feedback regions are located over the climate transition zones, including India, Indochina-southeast China, and northeast China-southeast Mongolia regions along the oceanic basin where the correlation magnitude is almost greater than 0.7, while the elasticity is higher than 2.

2. Other variables, including T2m and PET, also influence the precipitation-runoff processes. The T2m-ROF exhibits negative signals over most part of the study area except the TP regions where it represents positive processes due to the higher topography and cold weather regime. The PET-ROF indicates negative response over most of part of the study area excluding India and north China-southeast Mongolia regions where the signals are positive which may be due to the dominant impact of land-atmosphere interactions rather than the local water balance over these regions.
3. The SM reflects high correlation with runoff, demonstrating the importance of SM in the P-ROF processes. The higher values for SM-ROF correlation mainly locate over the climate transition zones, including India and Indochina-southeast China regions.
4. The initial SM anomalies have a potential impact on the subsequent changes of ROF in spring, summer, and autumn seasons. The initial wet (dry) SM anomalies lead to the increase (decrease) of ROF in each season. The hot spots with significant changes of runoff are located in the middle to high latitudes (above 30°N) in spring, TP-Indochina and northeast regions in summer, and TP and northeast regions in autumn. By comparison, the persistence of influence can last longer in spring, almost 4 months in both the dry and wet conditions, while it is short in autumn (only 1 month); the wet condition has stronger influence at the beginning but dissipates quickly, while the dry condition can last longer in the same season. Consistently, these regions also have significant changes of ET, P, or T2m.
5. The impact of initial ST anomalies is weaker on the subsequent runoff processes as compared to the initial SM anomalies. However, there are few regions where the ST has significant influence on runoff, for example, south China in spring (in warmer condition) and summer, and north India region in autumn.

**Acknowledgments**

We very much appreciate the Editor and three reviewer's valuable comment that helped us to improve the manuscript. This study was supported by the United States Department of Agriculture (USDA) award 2015-68007-23210, the Fundamental Research Funds for the Central Universities of China (grants 2015B00214, 2015B28514), the Special Fund of State Key Laboratory of Hydrology-Water Resources (grant 20145027312) and the program of Innovative Research Team in Jiangsu Province, and the National Key R&D Program of China (grants 2016YFC0402701, 2016YFC0402706 and 2016YFC0402710). The GLDAS data used in this study were acquired as part of the mission of NASA's Earth Science Division and archived and distributed by the Goddard Earth Sciences (GES) Data and Information Services Center (DISC) (http://disc.sci.gsfc.nasa.gov/services/grads-gds/gldas).

## References

Andréassian, V., Ü. Mander, and T. Pae (2016), The Budyko hypothesis before Budyko: The hydrological legacy of Evald Oldekop, *J. Hydrol.*, *535*, 386–391.

Anthes, R. A. (1977), A cumulus parameterization scheme utilizing a one-dimensional cloud model, *Mon. Weather Rev.*, *105*(3), 270–286.

Arnault, J., S. Wagner, T. Rummler, B. Fersch, J. Bliefernicht, S. Andresen, and H. Kunstmann (2016), Role of runoff–infiltration partitioning and resolved overland flow on land–atmosphere feedbacks: A case study with the WRF-Hydro coupled modeling system for west africa, *J. Hydrometeorol.*, *17*, 1489–1516.

Beltrami, H. (2001), On the relationship between ground temperature histories and meteorological records: A report on the Pomquet station, *Global Planet. Change*, *29*(3–4), 327–348.

Beltrami, H., and L. Kellman (2003), An examination of short- and long-term air-ground temperature coupling, *Global Planet. Change*, *38*(3–4), 291–303.

Bouchet, R. (1963), Evaporation re'elle et potentielle, signification climatique, in *General Assembly Berkeley*, Publ. 62, pp. 134–142, Int. Assoc. Sci. Hydrol., Gentbrugge, Belgium.

Brikowski, T. H. (2015), Applying multi-parameter runoff elasticity to assess water availability in a changing climate: an example from Texas, USA, *Hydrol. Processes*, *29*, 1746–1756.

Brubaker, K. L., and D. Entekhabi (1996), Analysis of feedback mechanisms in land-atmosphere interaction, *Water Resour. Res.*, *32*(5), 1343–1357, doi:10.1029/96WR00005.

Budyko, M. I. (1974), *Climate and Life*, *International Geophysics Series*, vol. 18, pp. 508, Academic Press, New York.

Chattopadhyay, S., and D. R. Edwards (2016), Long-term trend analysis of precipitation and air temperature for Kentucky, United States, *Climate*, *4*, 10.

Chiew, F. H. S. (2006), Estimation of rainfall elasticity of streamflow in Australia, *Hydrol. Sci. J.*, *51*(4), 613–625.

Cong, Z., D. Yang, B. Gao, H. Yang, and H. Hu (2009), Hydrological trend analysis in the Yellow River Basin using a distributed hydrological model, *Water Resour. Res.*, *45*, W00A13, doi:10.1029/2008WR006852.

Dickinson, R. E., A. Henderson-Sellers, and P. J. Kennedy (1993), Biosphere atmosphere transfer scheme (BATS) version 1E as coupled to the NCAR Community Climate Model NCAR. Tech Note. NCAR-383+str.

Dirmeyer, P. A. (2011), The terrestrial segment of soil moisture-climate coupling, *Geophys. Res. Lett.*, *38*, L16702, doi:10.1029/2011GL048268.

Donohue, R. J., M. L. Roderick, and T. R. McVicar (2011), Assessing the differences in sensitivities of runoff to changes in climatic conditions across a large basin, *J. Hydrol.*, *406*(3–4), 234–244.

Dooge, J. C. I., M. Bruen, and B. Parmentier (1999), A simple model for estimating the sensitivity of runoff to long-term changes in precipitation without a change in vegetation, *Adv. Water Resour.*, *23*, 153–163.

Elguindi, N., X. Q. Bi, F. Giorgi, B. Nagarajan, J. Pal, F. Solmon, S. Rauscher, A. Zakey and G. Giuliani (2011), Regional climatic model RegCM user manual version 4.1, The Abdus Salam International Centre for Theoretical Physics Strada Costiera, Trieste.

Emanuel, K. A. (1991), A scheme for representing cumulus convection in large-scale models, *J. Atmos. Sci.*, *48*(21), 2313–2329.

Emanuel, K. A., and M. Zivkovic-Rothman (1999), Development and evaluation of a convection scheme for use in climate models, *J. Atmos. Sci.*, *56*(11), 1766–1782.

Entekhabi, D., I. Rodriguez-Iturbe, and R. L. Bras (1992), Variability in large-scale water balance with land surface-atmosphere interaction, *J. Clim.*, *5*(8), 798–813.
Fritsch, J. M., and C. F. Chappell (1980), Numerical prediction of convectively driven mesoscale pressure systems. Part 1: convective parameterization, *J. Atmos. Sci.*, *37*(8), 1722–1733.
Giorgi, F., et al. (2012), RegCM4: Model description and preliminary tests over multiple CORDEX domains, *Clim. Res.*, *52*, 7–29.
Gocic, M., and S. Trajkovic (2013), Analysis of changes in meteorological variables using Mann-Kendall and Sen's slope estimator statistical tests in Serbia, *Global Planet. Change*, *100*, 172–182.
Grell, G. A. (1993), Prognostic evaluation of assumptions used by cumulus parameterizations, *Mon. Weather Rev.*, *121*, 764–787.
Grell, G. A., J. Dudhia, and D. R. Stauffer (1994), A description of the fifth generation penn state/NCAR mesoscale model (MM5). NCAR Technical Note NCAR/TN-398+STR.
Guo, Z. C., P. A. Dirmeyer, R. D. Koster, G. Bonan, E. Chan, and P. Cox (2006), GLACE: The global land-atmosphere coupling experiment. Part II: Analysis, *J. Hydrometeorol.*, *7*, 611–625.
Helama, S., H. Tuomenvirta, and A. Venalainen (2011), Boreal and subarctic soils under climatic change, *Global Planet. Change*, *79*(1–2), 37–47.
Holtslag, A. A. M., E. I. F. C. Bruijin, and H. L. Pan (1990), A high resolution air mass transformation model for short-range weather forecasting, *Mon. Weather Rev.*, *118*, 1561–1575.
Huang, Z., and H. Yang (2015), Dominant climatic factor driving annual runoff change at catchments scale over China, *Hydrol. Earth Syst. Sci. Discuss.*, *12*, 12,911–12,945.
Intergovernmental Panel on Climate Change (2007a), *Climate Change 2007*, Working Group II Contribution to the Fourth Assessment Report of the IPCC Intergovernmental Panel on Climate Change, Cambridge Univ. Press, Cambridge, New York.
Intergovernmental Panel on Climate Change (2007b), *Climate Change 2007*, Working Group I Contribution to the Fourth Assessment Report of the IPCC Intergovernmental Panel on Climate Change, Cambridge Univ. Press, Cambridge, New York.
Jiang, T., Y. D. Chen, C. Y. Xu, X. Chen, X. Chen, and V. P. Singh (2007), Comparison of hydrological impacts of climate change simulated by six hydrological models in the Dongjiang Basin, south China, *J. Hydrol.*, *336*, 316–333.
Kalnay, E., et al. (1996), The NCEP/NCAR 40-year reanalysis project, *Bull. Am. Meteorol. Soc.*, *77*, 437–471.
Kanamistu, M., W. Ebisuzaki, and J. Woollen (2002), NCEP-DOE AMIP-II reanalysis (R-2), *Bull. Am. Meteorol. Soc.*, *83*, 1631–1643.
Kendall, M., and J. D. Gibbons (1990), *Correlation Methods*, pp. 35–38, Oxford Univ. Press, Oxford.
Khedun, C. P., A. K. Mishra, J. D. Bolten, H. K. Beaudoing, R. A. Kaiser, J. R. Giardino, and V. P. Singh (2012), Understanding changes in water availability in the Rio Grande/Río Bravo del Norte basin under the influence of large-scale circulation indices using the Noah land surface model, *J. Geophys. Res.*, *117*, D05104, doi:10.1029/2011JD016590.
Kiehl, J. T., J. J. Hack, G. B. Bonan, B. A. Boville, B. P. Briegleb, D. L. Williamson, and P. J. Rasch (1996), Description of the NCAR Community Climate Model (CCM3). National Center for Atmospheric Research.
Konapala, G., and A. K. Mishra (2016), Three-parameter-based streamflow elasticity model: Application to MOPEX basins in the USA at annual and seasonal scales, *Hydrol. Earth Syst. Sci.*, *20*, 2545–2556.
Koster, R. D., and M. J. Suarez (1999), A simple framework for examining the interannual variability of land surface moisture fluxes, *J. Clim.*, *12*(7), 1911–1917.
Koster, R. D., Z. C. Guo, P. A. Dirmeyer, G. Bonan, E. Chan, and P. Cox (2006), GLACE: The global land-atmosphere coupling experiment. Part I: Overview, *J. Hydrometeorol.*, *7*, 590–610.
Koster, R. D., S. P. P. Mahanama, T. J. Yamada, et al. (2011), The second phase of the Global Land-Atmosphere Coupling Experiment: Soil moisture contributions to subseasonal forecast skill, *J. Hydrometeorol.*, *12*(5), 805–822.
Li, H. Y., M. Sivapalan, and F. Q. Tian (2012), Comparative diagnostic analysis of runoff generation processes in Oklahoma DMIP2 basins: The Blue River and the Illinois River, *J. Hydrol.*, *418–419*, 90–109.
Liu, D., G. L. Wang, R. Mei, Z. B. Yu, and H. H. Gu (2014a), Diagnosing the strength of land-atmosphere coupling at sub-seasonal to seasonal time scales in Asia, *J. Hydrometeorol.*, *15*, 320–339.
Liu, D., G. L. Wang, R. Mei, Z. Yu, and M. Yu (2014b), Impact of initial soil moisture anomalies on climate mean and extremes over Asia, *J. Geophys. Res. Atmos.*, *119*, 1–14, doi:10.1002/2013JD020890.
Liu, D., Z. Yu, and J. Y. Zhang (2015), Diagnosing the strength of soil temperature in the land-atmosphere interactions over Asia based on RegCM4 model, *Global Planet. Change*, *130*, 7–21.
Liu, X., X. J. Zhang, Q. Tang, and X. Z. Zhang (2014), Effects of surface wind speed decline on modeled hydrological conditions in China, *Hydrol. Earth Syst. Sci.*, *18*, 2803–2813.
Livneh, B., and D. P. Lettenmaier (2010), Noah LSM snow model diagnostics and enhancements, *J. Hydrometeorol.*, *11*, 721–738.
Ma, H., D. Yang, S. K. Tan, B. Gao, and Q. Hu (2010), Impact of climate variability and human activity on streamflow decrease in the Miyun Reservoir catchment, *J. Hydrol.*, *389*, 317–324.
Ma, Y., S. Kang, L. Zhu, B. Xu, L. Tian, and T. Yao (2008), Tibetan observation and research platform-atmosphere-land interaction over a heterogeneous landscape, *Bull. Am. Meteorol. Soc.*, *89*, 1487–1492.
Mishra, A. K., and V. P. Singh (2010), Changes in extreme precipitation in Texas, *J. Geophys. Res.*, *115*, D14106, doi:10.1029/2009JD013398.
Mishra, A. K., V. P. Singh, and M. Özger (2011), Seasonal streamflow extremes in Texas river basins: Uncertainty, trends, and teleconnections, *J. Geophys. Res.*, *116*, D08108, doi:10.1029/2010JD014597.
Mitchell, K. (2001), The community Noah land-surface model (LSM). User's Guide, Public Release Version 2.7.1.
Mitchell, T. D., and P. D. Jones (2005), An improved method of constructing a database of monthly climate observations and associated high-resolution grids, *Int. J. Climatol.*, *25*, 693–712.
Nunes, J. P., J. Seixas, J. J. Keizer, and A. J. D. Ferreira (2009), Sensitivity of runoff and soil erosion to climate change in two Mediterranean watersheds. Part II: assessing impacts from changes in storm rainfall, soil moisture and vegetation cover, *Hydrol. Processes*, *23*, 1212–1220.
Oke, T. R. (1978), *Boundary Layer Climates*, pp. 372, John Wiley, New York.
Ol'dekop, E. M. (1911), On evaporation from the surface of river basins, *Trans. Meteorol. Observ.*, *4*, 200.
Oleson, K. W., G. Y. Niu, Z. L. Yang, D. M. Lawrence, P. E. Thornton, and P. J. Lawrence (2007), *CLM3. 5 Documentation*, pp. 34 , National Center for Atmospheric Research, Boulder, Colo.
Oleson, K. W., G. Y. Niu, Z. L. Yang, D. M. Lawrence, P. E. Thornton, and P. J. Lawrence (2008), Improvements to the Community Land Model and their impact on the hydrological cycle, *J. Geophys. Res.*, *113*, G01021, doi:10.1029/2007JG000563.
Potter, N. J., and F. H. S. Chiew (2011), An investigation into changes in climate characteristics causing the recent very low runoff in the southern Murray-Darling Basin using rainfall-runoff models, *Water Resour. Res.*, *47*, W00G10, doi:10.1029/2010WR010333.
Rayner, N. A., D. E. Parker, E. B. Horton, C. K. Rolland, L. V. Alexander, D. P. Rowell, E. C. Kent, and A. Kaplan (2006), UKMO—GISST/MOHMATN4/MOHSST6—Global Ice coverage and SST (1856–2006), *NCAS British Atmospheric Data Centre*.

Risbey, J. S., and D. Entekhabi (1996), Observed Sacramento basin streamflow response to precipitation and temperature changes and its relevance to climate impact studies, *J. Hydrol.*, *184*, 209–223.
Rodell, M., and P. R. Houser (2004), Updating a land surface model with MODIS-derived snow cover, *J. Hydrometeorol.*, *5*, 1064–1075.
Rodell, M., P. R. Houser, U. E. A. Jambor, and J. Gottschalck (2004), The global land data assimilation system, *Bull. Am. Meteorol. Soc.*, *85*, 381–394.
Sankarasubramanian, A., and R. M. Vogel (2003), Hydroclimatology of the continental United States, *Geophys. Res. Lett.*, *30*(7), 1363, doi:10.1029/2002GL015937.
Sankarasubramanian, A., R. M. Vogel, and J. F. Limbrunner (2001), Climate elasticity of streamflow in the United States, *Water Resour. Res.*, *37*(6), 1771–1781, doi:10.1029/2000WR900330.
Schaake, J. C. (1990), *From Climate to Flow*, chap. 8, pp. 177–206, John Wiley, New York.
Schaake, J. C., V. I. Koren, Q.-Y. Duan, K. Mitchell, and F. Chen (1996), Simple water balance model for estimating runoff at different spatial and temporal scales, *J. Geophys. Res.*, *101*, 7461–7475, doi:10.1029/95JD02892.
Seager, R., A. Tzanova, and J. Nakamura (2009), Drought in the Southeastern United States: Causes, variability over the last millennium, and the potential for future hydroclimate change, *J. Clim.*, *22*, 5021–5045.
Sen, P. K. (1968), Estimates of the regression coefficient based on Kendall's tau, *J. Am. Stat. Assoc.*, *63*, 1379–1389.
Seneviratne, S. I., T. Corti, E. L. Davin, M. Mirschi, E. B. Jaeger, I. Lehner, B. Orlowsky, and A. J. Teuling (2010), Investigating soil moisture climate interactions in a changing climate: A review, *Earth Sci. Rev.*, *99*(1), 125–161.
Sheffield, J., G. Goteti, and E. F. Wood (2006), Development of a 50-yr high-resolution global dataset of meteorological forcings for land surface modeling, *J. Clim.*, *19*(13), 3088–3111.
Steiner, A. L., J. S. Pal, S. A. Rauscher, J. L. Bell, N. S. Diffenbaugh, A. Boone, L. C. Sloan, and F. Giorgi (2009), Land surface coupling in regional climate simulations of the West African monsoon, *Clim. Dyn.*, *33*, 869–892.
Tabari, H., and P. Hosseinzadeh Talaee (2011), Temporal variability of precipitation over Iran: 1966–2005, *J. Hydro.*, *396*(3–4), 313–320.
Tang, Q., T. Oki, S. Kanae, and H. Hu (2007), The influence of precipitation variability and partial 20 irrigation within grid cells on a hydrological simulation, *J. Hydrometeorol.*, *8*, 499.
Taxak, A. K., A. R. Murumkar, and D. S. Arya (2014), Long term spatial and temporal rainfall trends and homogeneity analysis in Wainganga basin, Central India, *Weather Climate Extremes*, *4*, 50–61.
Vano, J. A., T. Das, and D. P. Lettenmaier (2012), Hydrologic sensitivities of Colorado River runoff to changes in precipitation and temperature, *J. Hydrometeorol.*, *13*(3), 932–949.
Wang, Z., Y. Shen, and L. Song (2013), Hydrologic response of the climatic change based on SWAT Model in Beijiang River Basin, *Meteorol. Environ. Res.*, *01*, 8–12.
Wu, W. R., and R. E. Dickinson (2004), Time scales of layered soil moisture memory in the context of land-atmosphere interaction, *J. Clim.*, *17*, 2752–2764.
Xu, X., B. R. Scanlon, K. Schilling, and A. Sun (2013a), Relative importance of climate and land surface changes on hydrologic changes in the US midwest since the 1930s: Implications for biofuel production, *J. Hydrol.*, *497*(0), 110–120.
Xu, X., H. Yang, D. Yang, and H. Ma (2013b), Assessing the impacts of climate variability and human activities on annual runoff in the Luan River Basin, China, *Hydrol. Res.*, *44*, 940–952.
Yang, D., S. Herath, and K. Musiake (2000), Comparison of different distributed hydrological models for characterization of catchment spatial variability, *Hydrol. Processes*, *14*, 403–416.
Yang, D., F. Sun, Z. Liu, Z. Cong, and Z. Lei (2006), Interpreting the complementary relationship in non-humid environments based on the Budyko and Penman hypotheses, *Geophys. Res. Lett.*, *33*, L18402, doi:10.1029/2006GL027657.
Yang, H., and D. Yang (2011), Derivation of climate elasticity of runoff to assess the effects of climate change on annual runoff, *Water Resour. Res.*, *47*, W07,526, doi:10.1029/2010WR009287.
Yang, H., J. Qi, X. Xu, D. Yang, and H. Lv (2014), The regional variation in climate elasticity and climate contribution to runoff across China, *J. Hydrol.*, *517*, 607–616.
Zhang, J. Y., L. Y. Wu, and W. J. Dong (2011), Land-atmosphere coupling and summer climate variability over East Asia, *J. Geophys. Res.*, *116*, D05117, doi:10.1029/2010JD014714.
Zheng, H., L. Zhang, R. Zhu, C. Liu, Y. Sato, and Y. Fukushima (2009), Responses of streamflow to climate and land surface change in the headwaters of the Yellow River Basin, *Water Resour. Res.*, *45*, W00A19, doi:10.1029/2007WR006665.